remote sensing

MDPI

Article

A Multi-Disciplinary Approach to the Study of Large Rock Avalanches Combining Remote Sensing, GIS and Field Surveys: The Case of the Scanno Landslide, Italy

Mirko Francioni [1,2,*], Fernando Calamita [1], John Coggan [2], Andrea De Nardis [1], Matthew Eyre [2], Enrico Miccadei [1,3], Tommaso Piacentini [1,3], Doug Stead [4] and Nicola Sciarra [1]

1 Department of Engineering and Geology, University "G. d'Annunzio" of Chieti-Pescara, 66100 Chieti, Italy
2 Camborne School of Mines, University of Exeter, Penryn TR10 9EZ, Cornwall, UK
3 Istituto Nazionale di Geofisica e Vulcanologia, Sezione Roma 1, 00143 Rome, Italy
4 Department of Earth Sciences, Simon Fraser University, Burnaby, BC V5A 1S6, Canada
* Correspondence: mirko.francioni@unich.it

Received: 6 June 2019; Accepted: 30 June 2019; Published: 2 July 2019

Abstract: This research aims to highlight the importance of adopting a multi-disciplinary approach to understanding the factors controlling large rock avalanches using the Scanno landslide, Italy, as a case study. The study area is the Mount Genzana, Abruzzi Central Apennines, characterized by the regional Difesa-Mount Genzana-Vallone delle Masserie fault zone. The Scanno landslide is famous for its role in the formation of the Scanno Lake. The landslide is characterized by a wide exposed scar, which was interpreted in previous studies as the intersection of high-angle joints and an outcropping bedding plane on which the landslide failed sometime between the Upper Pleistocene and the Holocene. In this study, the Scanno landslide was investigated through the integration of geological, geomechanical and geomorphological surveys. Remote sensing techniques were used to enrich the conventionally gathered datasets, while Geographic Information Systems (GIS) were used to integrate, manage and investigate the data. The results of the authors investigation show that the outcropping landslide scar can be interpreted as a low-angle fault, associated with the Difesa-Mount Genzana-Vallone delle Masserie fault zone, which differs from previous investigations and interpretations of the area. The low-angle fault provides the basal failure surface of the landslide, with two systematic high-angle joint sets acting as lateral release and back scarp surfaces, respectively. In light of these new findings, pre- and post-failure models of the area have been created. The models were generated in GIS by combining LiDAR (Light Detection and Ranging) and geophysics data acquired on the landslide body and through bathymetric survey data of the Scanno Lake. Using the pre- and post-failure models it was possible to estimate the approximate volume of the landslide. Finally, back-analyses using static and dynamic limit equilibrium methods is also used to show the possible influence of medium-to-high magnitude seismic events in triggering the Scanno landslide.

Keywords: Scanno landslide; LiDAR; geological model; back-analysis; landslides in fault-zones; central Apennines

1. Introduction

Landslides are among the most dangerous natural disasters in mountainous areas. Rockfalls are associated with failures of single (or a small number of) blocks detaching from a slope, while rock avalanches involve large rock slope sections, with the failure/shear surface located at some depth below the ground surface. Through the statistical analysis of rockfall volume distributions, Dussauge [1]

provided a more precise definition of rockfall and rock avalanches, suggesting that the term rockfall is usually used to describe small phenomena, ranging in size from block falls of a few dm^3 up to 104 m^3 events. Rockslides sometimes involve more than 105 m^3, and rock avalanches can reach several million cubic meters. The occurrence of rock avalanches can be catastrophic and may result in damage to infrastructure or, in some cases, damming of rivers. This was the case for the Scanno landslide, which dammed the Tasso River forming the Scanno Lake in the early 900s [2]. This is one of the most famous examples of a naturally dammed lake in Italy (Figure 1).

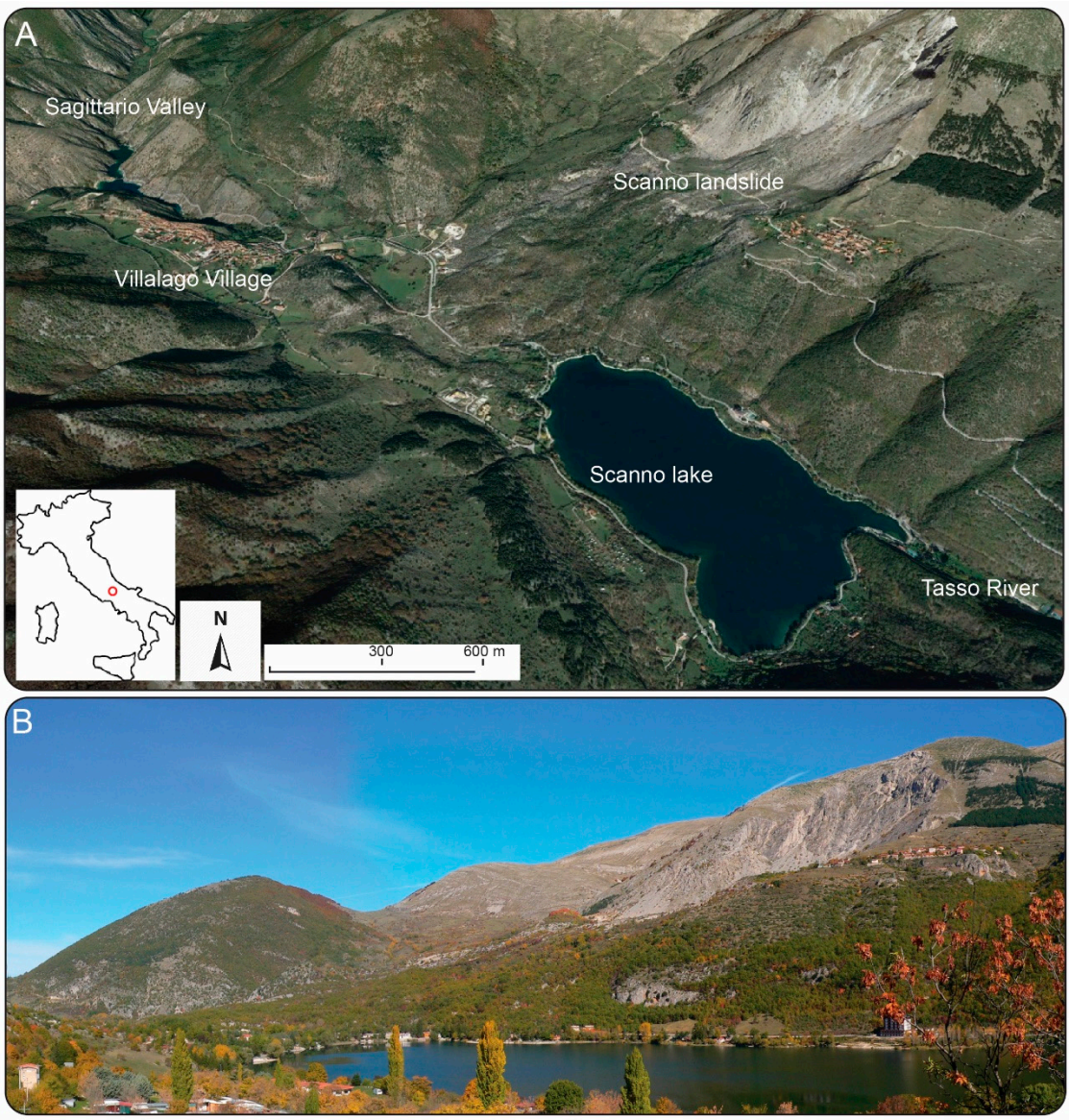

Figure 1. (**A**) Study area with the Scanno Lake, the Scanno landslide is highlighted with the geographic location of the area provided in the inset map. (**B**) Panoramic view of the Scanno landslide that dammed the Tasso River forming the Scanno Lake (view from south).

The Scanno landslide has been investigated in several previous studies over the last few decades. Nicoletti et al. [3] described the geometry of the landslide, with particular focus on the debris accumulation area and deposition mechanisms. More recently, Bianchi-Fasani et al. [4] and Della Seta et al. [5], described the Scanno landslide as a slow-moving rock avalanche where the bedding planes represent the sliding surface. Radiocarbon dating of soil samples collected from the landslide debris accumulation has suggested an age of c. 12,800 years [4]. Bianchi-Fasani et al. [4] focused their

analysis on the study of landslide debris/dams, highlighting the importance of the geological model in the analysis of the factors controlling the life-span of a rockslide dam. The authors verified the good stability condition of the Scanno rockslide dam, favored by the high volume of debris and the small dam height to the length ratio value. Della Seta et al. [5] proposed a new mid-term landscape evolutionary model of the Mt. Genzana calcareous ridge. Such a model was used by the authors to (i) back analyze the landslide, (ii) highlight the importance of rock mass creep during some stage of the morpho-evolution of the valley, and (iii) verify the role of the inherited structural pattern in the identification of preferential strain concentration zones and failure surfaces along bedding planes.

In this research, a different geological model developed through the integration of the results of geological, geomechanical and geomorphological surveys, is proposed. Our results highlight that the outcropping Scanno landslide scar can be defined as a combination of a low-angle normal fault associated with the Difesa-Mount Genzana-Vallone delle Masserie (DMG) fault zone, and two main high-angle joint sets. The low-angle fault likely provided the basal failure surface during the rock avalanche that generated the lake, with the two main joint sets representing the lateral release surfaces and tension cracks. The main joint sets and the geometrical characteristics of the landslide have been studied by integrating the results from conventional geomorphological, geomechanical and structural surveys, with data from Digital Photogrammetry (DP) and LiDAR (Light Detection and Ranging) analyses.

Structural and geomechanical surveys are usually the first step in the analysis of rock slopes [6–10]. Using this approach, it is possible to understand the characteristics of rock masses and the kinematic relationship between the rock slope and discontinuities. However, when dealing with non-accessible areas, the integration of these surveys with more innovative remote sensing techniques can provide more accurate characterization and definition of the rock slopes being investigated [11–14]. The benefits of integration of geomechanical survey and DP data has been explored by several authors [15–18]. Ferrero et al. [15] analyzed rock cliff hazards in the Lake Garda (Italy) through remote geostructural surveys while Francioni et al., [16,17] used DP data to provide improved understanding of the role of structure on erosion of inaccessible rocky coastlines in Cornwall (UK) and the analysis of heterogeneous rock masses in the Italian Central Apennines. Rossi et al. [18] illustrated the potential use of multitemporal UAV for landslide mapping and characterization while Calista et al. [19] combined geomorphological, geostructural and UAV data with numerical modelling in the analysis of weak rock landslides in Central Italy. Riquelme et al. [20] proposed a method of undertaking rock mass characterization based on the analysis of LiDAR and DP generated point clouds. A review of advantages and limitations of remote sensing techniques in the study of rock slopes was also highlighted by Zhao and Lu [21].

For this study, data obtained from geological and geomechanical surveys were integrated with an in-depth geomorphological analysis of the area, carried out using both field and LiDAR data. Geographic Information Systems (GIS) were used to manage all the data, to create thematic maps and to improve the interpretation of geological features. The integrated use of LiDAR data and GIS in the study of landslides has been highlighted by several authors in recent years [5,22–25]. An excellent review on the use of LiDAR techniques in landslide investigations has been provided by Jaboyedoff et al. [26].

Once the geometry of the Scanno landslide scar was established, geophysical data (collected in the landslide accumulation area) was used and bathymetric profiles of the Scanno Lake obtained, allowing improved understanding of geometry the paleo-valley. Using this approach, it was possible to develop pre- and post-failure 3D landslide models of the area, which provided the basis to calculate the likely volume of the landslide through change detection analyses. Based on these results, limit equilibrium analyses were performed assuming both static and dynamic conditions, using the data available from the seismic risk map of Italy [27].

The multi-disciplinary approach applied in this research has improved the geological model of the area and allowed construction of a kinematic model of the Scanno landslide. The results demonstrate the importance of an integrated approach and the key role of geological-structural models in the analysis of large rock avalanches.

2. Study Area

The Scanno landslide is located in the Tasso Stream and Sagittario River drainage basin, downstream from the Scanno Lake, between the Montagna Grande and Mt. Genzana ridges. It is in one of the highest average elevation areas in the entire Central Apennines. The valley runs parallel to one of the main drainage divides of the region, between the Fucino endorheic basin and the Adriatic piedmont and coastal area (Figure 2) [28–30].

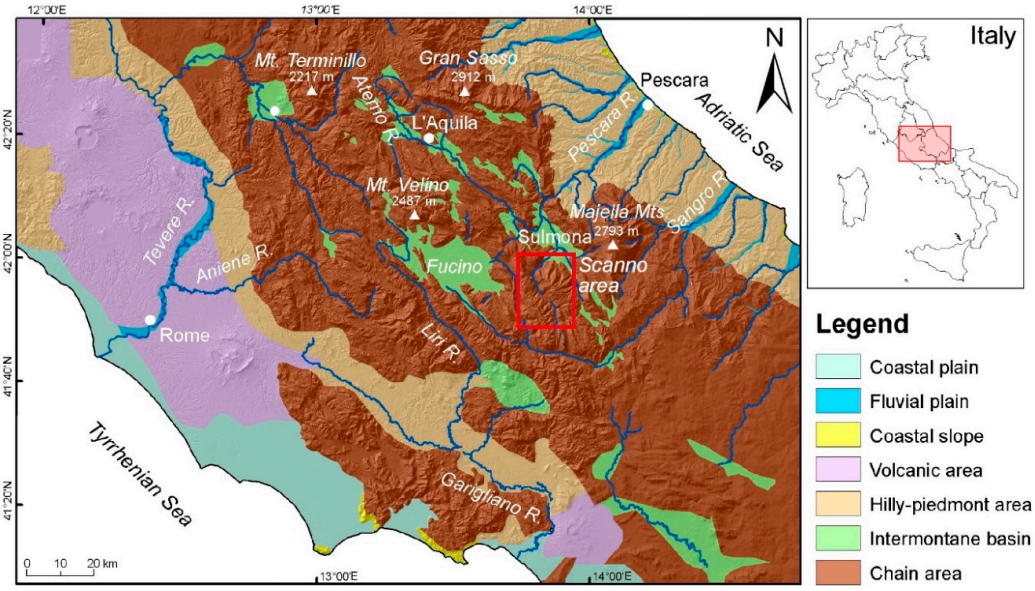

Figure 2. Location map of the study area within the physiographic setting of Central Italy, modified from Reference [22]. The study area is located in the red box.

The main valley is deeply incised into a pelitic-arenaceous bedrock representing Neogene foredeep sequences [31]. The eastern margin of the Lazium-Abruzzo carbonate shelf is tectonically juxtaposed to the calcareous-marly Mount Genzana slope-to-basin domain along a major NNW-SSE tectonic lineament (Profluo-Tasso-Sagittario line), which includes the DMG fault zone [31–36]. From the late Miocene onwards, the above-mentioned domains have been affected by deformation which resulted in: (i) pre-thrusting normal faulting related to foreland flexural processes (DMG fault); (ii) pervasive faulting combining Late Miocene–Early Pliocene thrusting (Montagna Grande thrust); (iii) Pliocene strike-slip tectonics (DMG fault); (iv) Pleistocene normal faulting (local reactivation of the DMG fault in the Scanno area). During the Quaternary, the landscape was deeply incised following regional uplift with local base level variations [37]. In addition, sequences of glacial, slope, alluvial fan and fluvial continental deposits have blanketed the bedrock [31].

The overall landscape is characterized by wide valleys in which deep incisions and gorges were carved (Figure 3), which can be related to the tectonically induced drops in the base level of the Sulmona basin. The area is largely characterized by structurally controlled landforms and fluvial landforms related to the incision, whereas, the highest elevations areas (1500 m a.s.l.) are largely affected by karst landforms and glacial features (inherited during the Pleistocene glacial stages) [29].

The main distinctive element in the geomorphological architecture of the basin is the Scanno landslide. This is a large rock avalanche, from 86 to 90 $\times$ 10^6 m^3 of limestone and subordinate flysch according to Nicoletti et al. [1] and Bianchi-Fasani et al. [4], detached from the eastern side of the main valley (Mt. Genzana). The landslide dammed the upper part of the valley causing the impoundment of Scanno Lake, and separation of the valley into two main branches; the southern Tasso valley and the northern Sagittario valley. The Scanno area has been previously studied by several authors [3–5,38]. Della Seta et al. [5] proposed an interpretation of the morpho-structural evolution of

the valley-slope systems with related implications for slope gravitational processes. They interpreted the landslide as a slow-moving rock avalanche in which the bedding planes represented the sliding surface. Bianchi-Fasani et al. [4] proposed a similar geological model in the analysis of the life-span of the Scanno landslide-dam. Bianchi-Fasani et al. [4] performed a geophysical survey of the valley to improve the understanding of the paleo-valley morphology (Figure 4A). In 2014, Carmisciano et al. [38] presented the results of a geophysical/bathymetric survey carried out in the lake indicating that 'strange phenomena'/electromagnetic anomalies were observed on the site (Figure 4B).

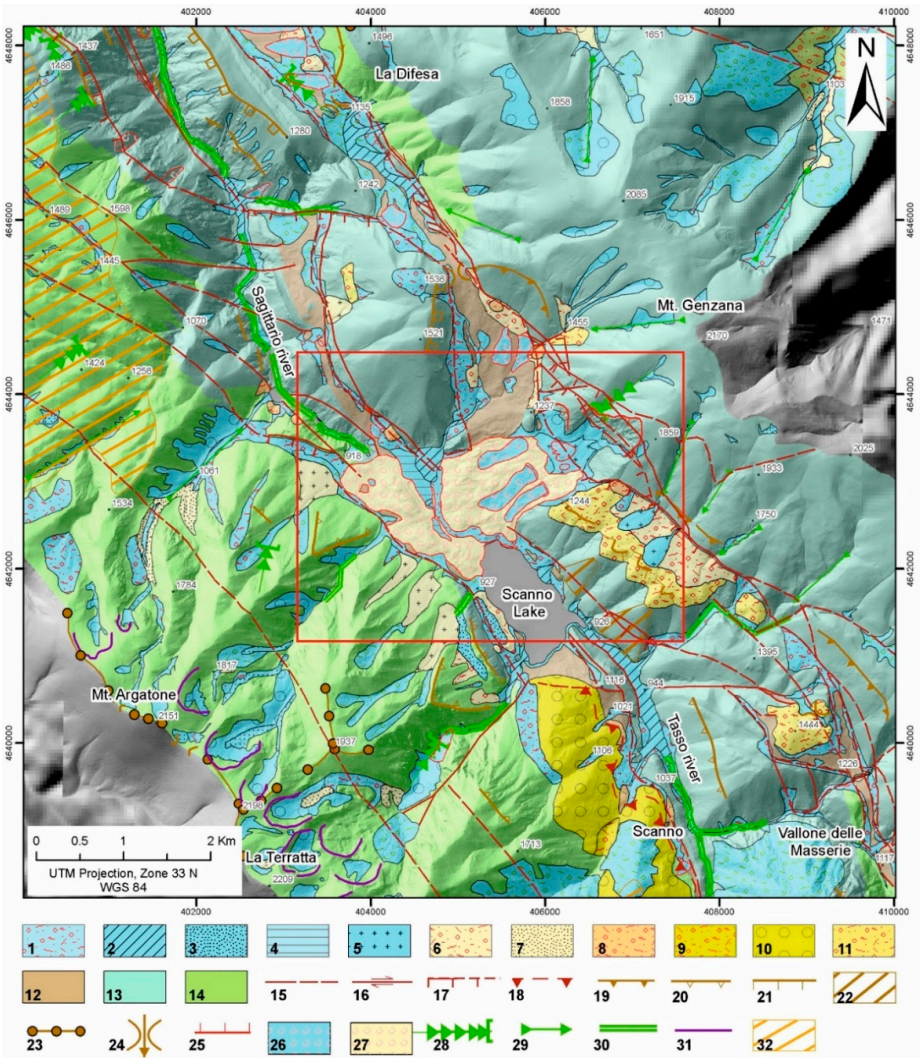

Figure 3. Geological and geomorphological map of the Scanno landslide area (modified from Miccadei, [29]; ISPRA, [31]; Miccadei et al. [33]). The Scanno landslide is located in the red box. Legend: Holocene: (1) talus slope deposits; (2) alluvial fan deposits; (3) colluvial deposits; (4) palustrine deposits; (5) mixed slope-alluvial fan deposits. Upper Pleistocene: (6) slope deposits; (7) mixed deposits. Middle Pleistocene: (8) slope deposits. Lower Pleistocene: (9) slope deposits (upper unit); (10) fluvial-alluvial fan deposits (upper unit); (11) slope deposits (lower unit). Bedrock: (12) Neogene pelitic-arenaceous siliciclastic rocks; (13) Jurassic-Paleogene limestone and marly-limestone; (14) Jurassic-Miocene limestone. Tectonics: (15) fault (dashed if uncertain or buried); (16) strike-slip fault; (17) normal fault (dashed if uncertain or buried); (18) thrust (dashed if uncertain or buried). Geomorphology: (19) fault scarp; (20) fault line scarp; (21) structural scarp; (22) triangular facet; (23) ridge; (24) windgap; (25) landslide scarp; (26) recent landslide; (27) landslide; (28) hanging valley; (29) rectilinear valley; (30) gorge; (31) glacial cirque; (32) karst area.

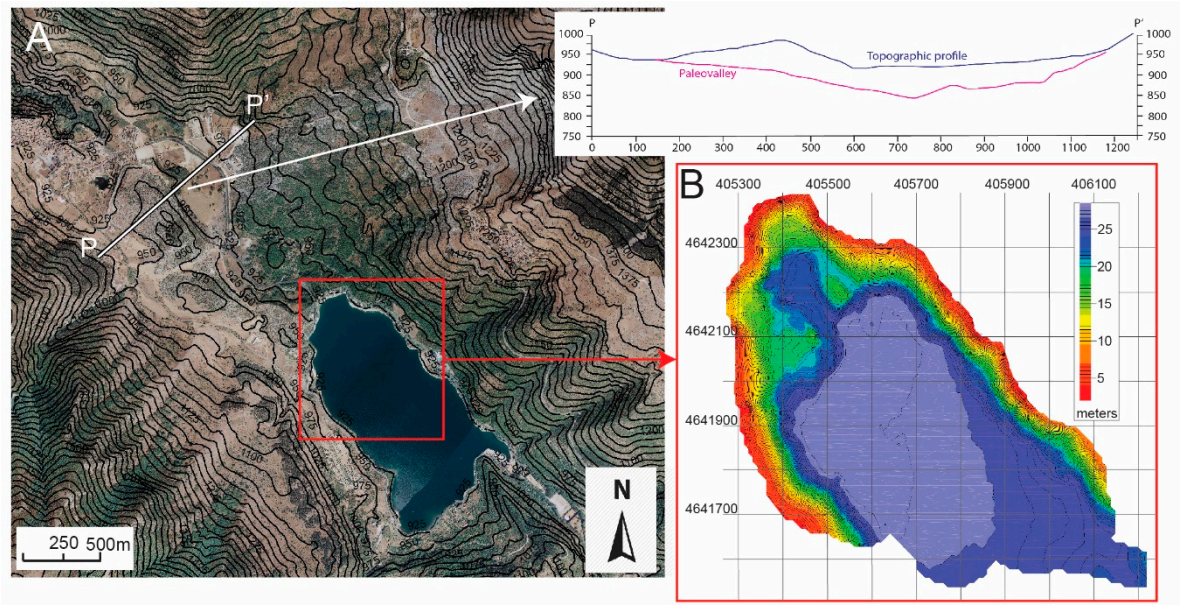

Figure 4. (**A**) Geophysical profile P-P′ through the orthophoto of the area and bathymetry of the Scanno Lake. After Bianchi-Fasani et al. [4]. (**B**) Bathymetry of the lake modified after Carmisciano et al. [39]

3. Materials and Methods

Geological, geomechanical and geomorphological surveys were undertaken to reconstruct the geological model of the selected areas. These were subsequently integrated with remote sensing surveys and GIS to improve the understanding of the factors controlling the landslide. Finally, using existing geophysics and bathymetric data, a reconstruction of pre- and post-failure models of the landslide was analysed using static and dynamic limit equilibrium analyses.

3.1. Geological and Geomorphological Surveys

Field-based and remote sensing analyses were conducted to understand the main lithologies, geological formations, discontinuity sets, faults and the distribution of the main landforms (focusing on the structural and gravity-induced landforms) outcropping in the area. The DMG fault zone was studied to provide an evaluation of fault damage zones, fault cores and kinematic indicators using the classification proposed by Sibson, [40]. Based on the Geological Survey guidelines [31], the geological and geomorphological surveys were conducted at 1:5000 scale with data at 1:1000 scale developed for the landslide scar area. Field investigations were combined with the study of aerial photographs, orthophoto and LiDAR data (Table 1), to improve the understanding of geological and geomorphological features (e.g., fault lineaments, talus cones, trenches, alluvial fans, landslide scar, etc.).

Table 1. Main aerial photograph and LiDAR data used in this work.

	Year	Resolution	Source
Aerial Photograph	2007	0.1 m	Open Geodata service Abruzzo Region (http://opendata.regione.abruzzo.it/)
Orthophoto	2013	0.5 m	Open Geodata service Abruzzo Region (http://opendata.regione.abruzzo.it/)
LiDAR data	2011	1 m	Ministry of Environment (NationalGeoportal,http://www.pcn.minambiente.it/)

3.2. Geomechanical and Digital Photogrammetry Analyses

Conventional geomechanical surveys were conducted to determine the characteristics of the main discontinuity sets (Figure 5A). However, due to the difficulties in accessing most of the outcrops

around the landslides, DP was used to improve the data obtained from conventional geomechanical surveys. The photogrammetric model was created using independent convergent methods [41] and five photogrammetric station locations (for a total of 35 photographs; Figure 5). The baseline between each station was c. 10 meters and the distance from the outcrop around 500 meters. The survey was carried out using a Nikon D5100 and 100, 150 and 200 mm focal length lenses. During the creation of the photogrammetric models, the model needs to be scaled and oriented; this was achieved using georeferenced targets within the images. In this research, 5 ground control points (GCPs), recognizable in both the LiDAR model and in the photographs acquired during the DP survey, were selected and used to georeferenced the DP model. Due to the different resolution between the LiDAR model and the photographs, the GCP were selected using easily recognizable geological features such points of intersection of major joints, or easily delineated rock blocks.

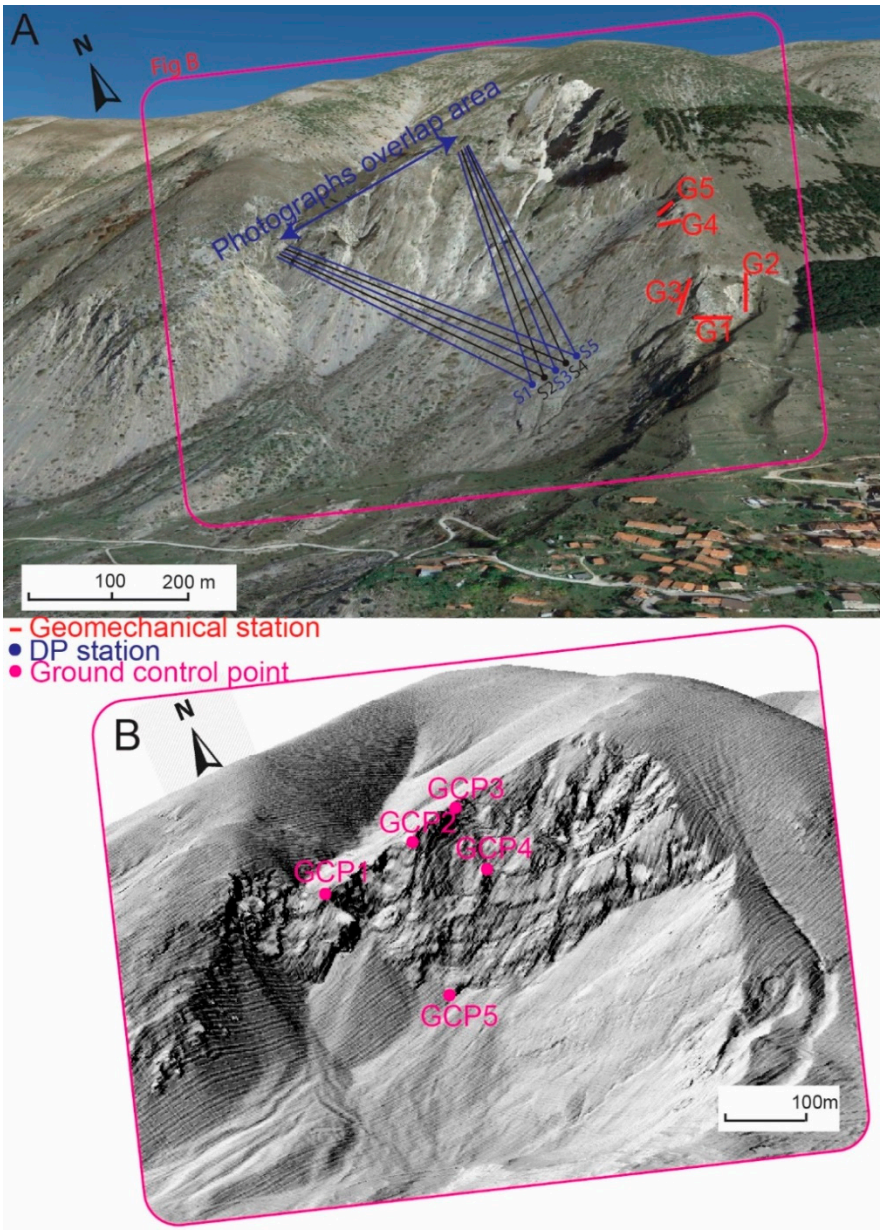

Figure 5. (**A**) 3D orthophoto model of the study area with highlighted geomechanical stations (G1–G5) and Digital Photogrammetry (DP) stations (S1-S5). (**B**) Ground control points extracted from the LiDAR and used for creating the DP model.

Figure 5A shows a 3D orthophoto of the study area with highlighted geomechanical stations (G1-G5) and DP stations (S1–S5); the ground control points extracted from the LiDAR are illustrated in Figure 5B. The integration of geomechanical survey and DP data aided in the definition of the attitude of the main joint sets and their geomechanical characteristics, and to define the Geological Strength Index (GSI) [42] in the different areas of the landslide scar.

3.3. GIS Analysis

Data obtained from the above-mentioned surveys was managed in a GIS platform. Thematic maps such as Hillshade, Slope and Aspect maps (Figure 6A–C) were extracted from the LiDAR DEM (Digital Elevation Model, Table 1). The maps were used to improve the understanding of the geological/geomorphic features and to create 3D pre- and post-failure geological models of the area.

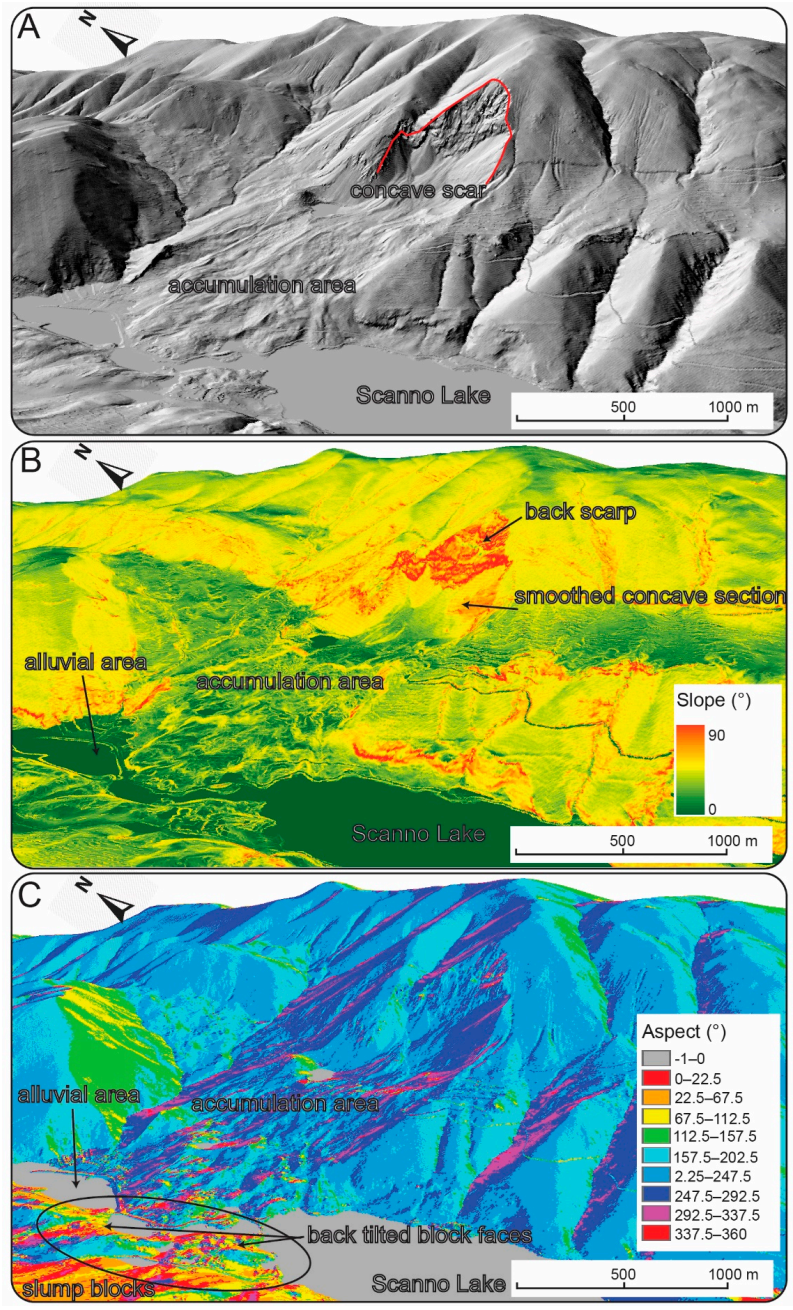

Figure 6. LiDAR-extracted GIS thematic maps of Scanno landslide. (**A**) Hillshade map. (**B**) Slope map. (**C**) Aspect map.

Geophysical data (Figure 4A, [4]) was used to estimate the thickness of the debris (depth of the bedrock) that dammed the lake (N-E side of the lake) while the bathymetric data of the Scanno Lake [35] was used to define the depth of the bedrock under the lake. Through integration of the geophysical and bathymetric data (Figure 4B), together with geological and geomorphological data, it was possible to infer the pre-failure contour and geometry of the valley.

The model obtained from this procedure, developed through ArcMap [43], was then compared with the current 3D model of the slope to calculate the landslide volume using the open source software CloudCompare [44].

This procedure highlighted both the areal extent and volume of the landslide. The volume of the landslide was estimated at around 100×10^6 m^3 and agrees with volume of the sediments associated with the landslide debris previously estimated by Scarascia Mugnozza et al. [38] (ca 96×10^6 m^3).

3.4. Kinematic and Limit Equilibrium Back-Analyses of the Landslide

The pre- and post-failure models and the geomechanical/structural information gained from conventional and remote sensing surveys were used to undertake a back-analysis of the landslide incorporating both kinematic and limit equilibrium approaches; the software used for this purpose were Dips v. 7, RocPlane v.3 and the newly developed 3D code Slide3 v.2 [45]. Through the kinematic analysis, it was possible to define the discontinuities acting as a potential failure surface, lateral release surfaces and tension cracks. The results of the kinematic analysis, provided the basis to perform a limit equilibrium simulation assuming both static and dynamic conditions. RocPlane was used to undertake an initial sensitivity analysis to understand the influence of friction angle and cohesion, using values ranging from 30° to 40° and from 0 to 0.2 MPa, respectively. The results of the sensitivity analysis were used to inform a probabilistic dynamic analysis, considering a range of seismic coefficients from 0.250 g to 0.275 g. The seismic coefficient was obtained from the Italian seismic hazard map [46] and is expressed in terms of PGA (Peak Ground Acceleration) with a probability of 10% exceedance in 50 years referring to rigid soils. According to the disaggregation of the seismic hazard [47], the PGA is most likely related to seismic events with a magnitude ranging from 4.5 to 6.5 occurring within 10 Km of the sites [46].

Based on results achieved in this analysis, a more detailed 3D limit equilibrium analysis using Slide3 has been performed. Slide3 allowed us to verify the results of limit equilibrium calculation using the observed slope geometry. The Slide3 3D model was developed by integrating the main discontinuities and landslide geometry obtained from the GIS analysis.

4. Results

4.1. Geological Model of the Study Area

The morphology of the landslide is characterized from the top to the bottom by a concave scar (elevation from 1860 m to 1175 m a.s.l.) and by a rugged accumulation or scree area with trapezoidal plan shape (elevation from 1275 m to 900 m a.s.l.) (Figure 6A). The scar shows a steep rugged back scarp (1860–1400 m a.s.l.), and a lower smoothed concave section (1400–1175 m a.s.l.) (Figure 6B). The landslide accumulation area features a gentle slope in the upper part (Figure 6B) with evidence of slump blocks (with back tilted faces) in the lower part along the valley bottom and upslope on the opposite valley side. The very bottom of the valley is represented by a flat alluvial area. The southernmost area of the landslide is submerged by the Scanno Lake (Figure 6B,C). Table 2 shows the main geometric characteristics of the landslide scar and the accumulation area.

Table 2. Areal extent and elevation of the landslide scar and accumulation area.

	Area (m^2)	Elevation max (m)	Elevation min (m)
Landslide scar	816,250	1860	1175
Landslide accumulation	2,750,600	1275	900

The landslide affected Jurassic-Paleogene marine limestone and marly-limestone with thin clayey-marly layers (Mount Genzana, MG, unit). The middle-lower part of the valley is formed by pelitic-arenaceous siliciclastic rocks (Neogene foredeep deposits). The bedrock is largely covered by Quaternary clastic continental deposits (slope breccia deposits, alluvial fan conglomerate) as well as the Scanno landslide. The latter is covered by more recent landslides (particularly in the NE flank of the valley) and by fluvial-alluvial fan deposits (in the bottom of the valley). Within the landslide scar, the bedrock is specifically covered by talus slope and cone deposits resulting from the recent degradation of the scar (Figure 7).

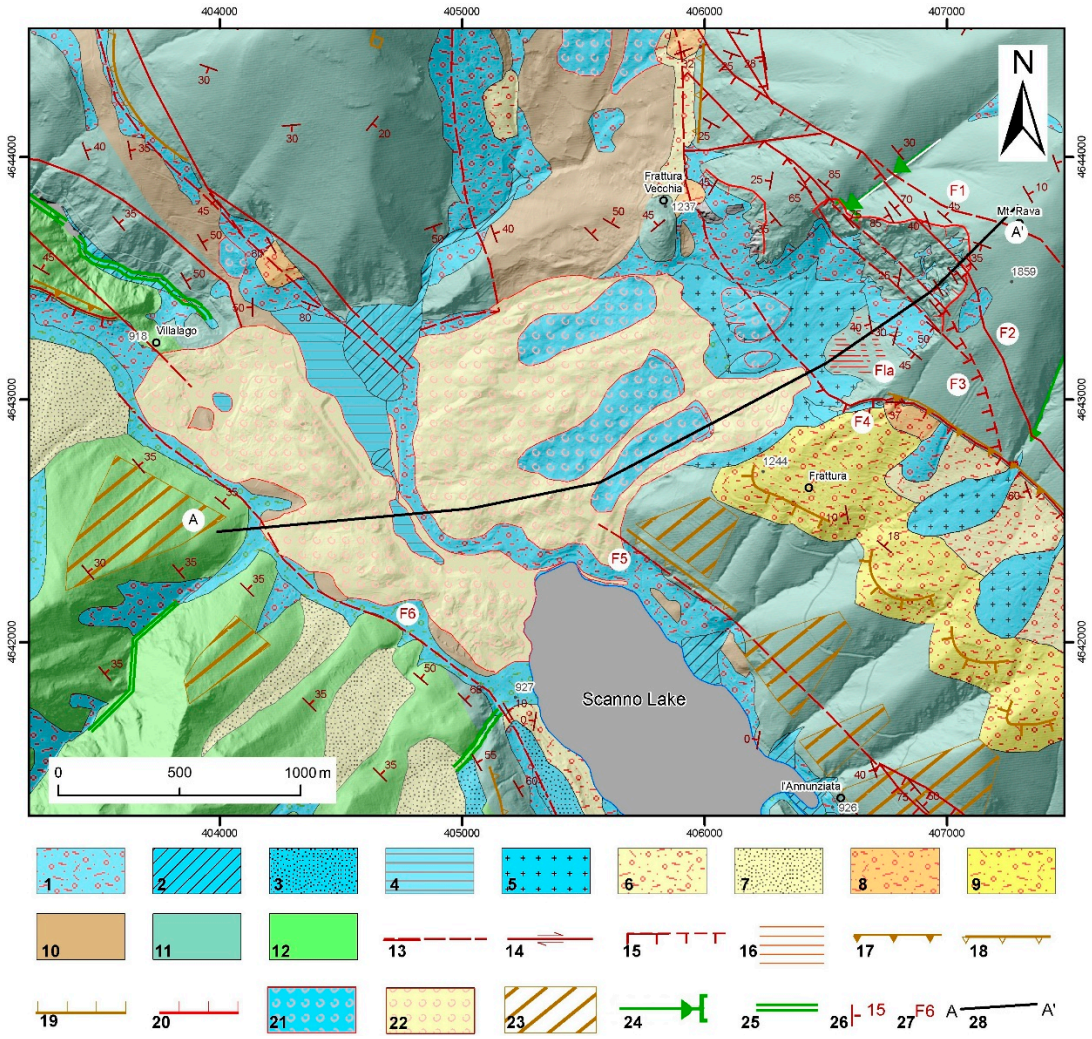

Figure 7. Geological and geomorphological map of the Scanno landslide area. Legend: Holocene: (1) talus slope deposits; (2) alluvial fan deposits; (3) colluvial deposits; (4) palustrine deposits; (5) mixed slope-alluvial fan deposits. Upper Pleistocene: (6) slope deposits; (7) mixed deposits. Middle Pleistocene: (8) slope deposits. Lower Pleistocene: (9) slope deposits. Bedrock: (10) Neogene pelitic-arenaceous siliciclastic rocks; (11) Jurassic-Paleogene limestone and marly-limestone; (12) Jurassic-Miocene limestone. Tectonics: (13) fault (dashed if uncertain or buried); (14) strike-slip fault; (15) normal fault (dashed if uncertain or buried). Geomorphology: (16) fault scarp; (17) fault line scarp; (18) structural scarp; (19) low-angle fault plane, Fla; (20) landslide scarp; (21) recent landslide; (22) landslide; (23) triangular facet; (24) hanging valley; (25) rectilinear valley; (26) strata attitude (number is the dip angle); (27) fault label; (28) Trace of geological and geomorphological cross-section.

The main DMG fault characterizes the area forming the tectonic contact between the MG unit (limestone and marly-limestone in the footwall) with siliciclastic deposits in the hanging-wall.

The bedrock attitude shows a homocline arrangement (dip direction equal to 40–50° and dip equal to 10–30°) in the Mount Genzana area; however, the attitude is very irregular in the fault zone (Figure 7). In the landslide area, the DMG fault zone consists of several main faults forming horse structures of different scale and sigmoidal geometries. Two main faults (F1 and F4 in Figure 7) envelop minor fault planes, including high-angle faults (F2, F3) and a low-angle fault plane (Fla, Figure 7). The kinematics of this fault zone are very complex, showing polyphasic deformation. A main normal dip-slip movement has been reconstructed by Agostini and Calamita [35] while strike-slip kinematics, identified from slickensides and sigmoidal structures, was documented by Corrado et al. [34] and ISPRA [31]. Two high-angle faults (F5, F6) bound the bottom of the valley, representing the tectonic contact between siliciclastic and carbonate bedrock.

The low-angle fault plane (Fla) (Figures 7 and 8A,B), has been interpreted in previous studies as an outcropping bedding plane [4,5,38].

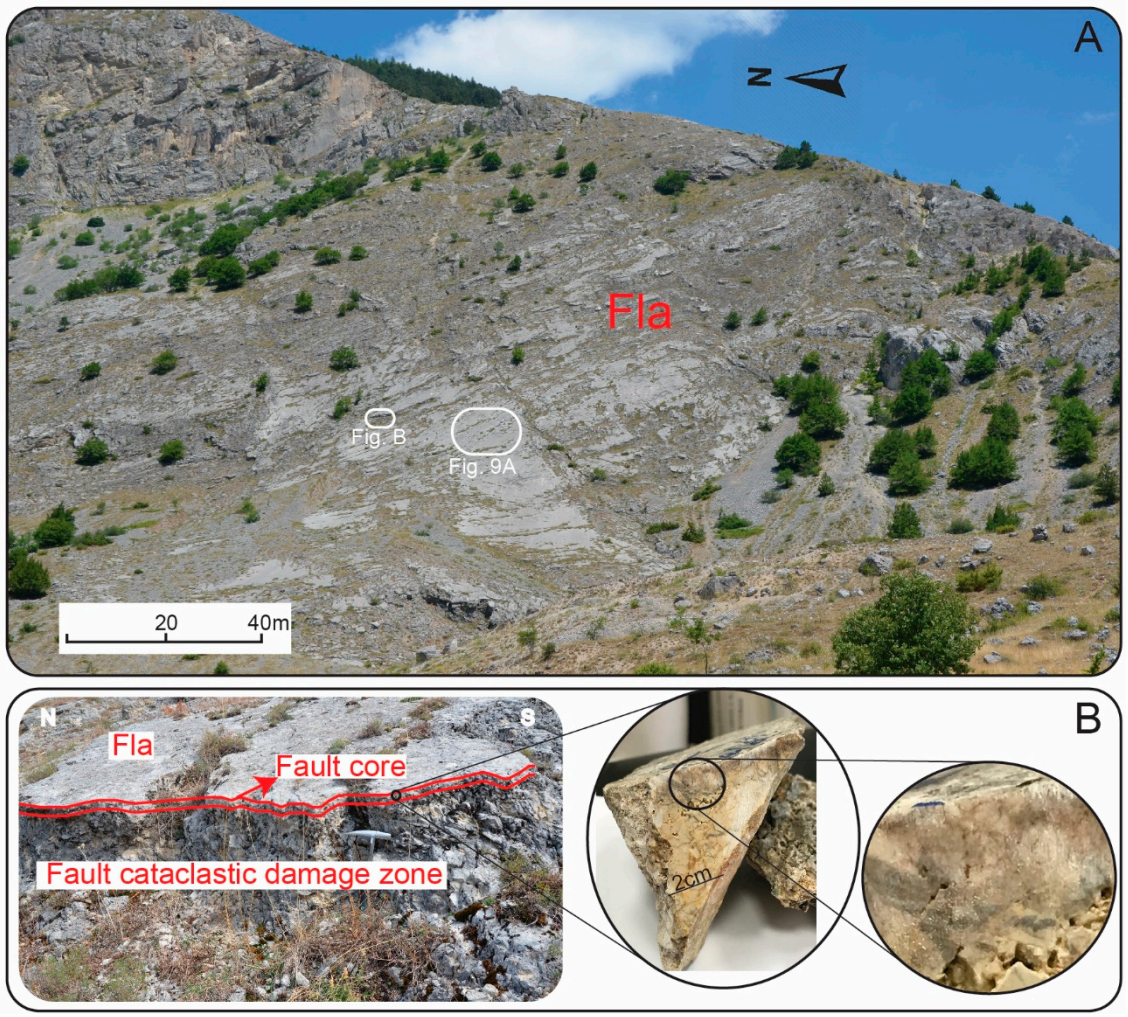

Figure 8. (**A**) Scanno landslide scar represented by a low-angle normal fault. (**B**) Fault core and damage zone in the fault zone and sample showing the fault rocks characterized by decreasing grain size in the proximity of the slip surface, combined with an increase of the percentage of the matrix, from crush breccia to cataclasite, in the fault core.

A targeted study has been undertaken along this surface. The surface has a mean dip direction of 250°, with a dip of up to 40° in the highest part and 25° in the lower part. The surface is characterized by 5 to 20 cm thick cohesive rock that overlies cataclastic fault rock (up to one meter thick). Such layers have been interpreted as a fault core and damage zone, respectively [37]. From this new information,

the surface has been interpreted as a low-angle normal fault (Fla) belonging to the DMG fault zone, which shows evidence of previous strike-slip kinematics [31]. This interpretation is supported by three further analyses:

(i) The analysis of samples collected in the fault core shows a decrease in grain size in close proximity to the slip surface, combined with an increase in the percentage of matrix (from crush breccia to cataclasite) (Figure 8B);

(ii) Synthetic Riedel shear planes have been identified on the main fault surface (Figure 9A). These structures have been reconstructed in 3D using DP (Figure 9B,C). The model created showed typical Riedel geometry with dip of the fault increasing approximately 15 degrees (from 30° to 45°) in the proximity of the shears (Figure 9C) [48];

(iii) The analysis of the main sliding surface of the landslide showed that it locally envelops low-angle intersecting fault planes forming metric to decametric sigmoidal geometries (Figure 9D);

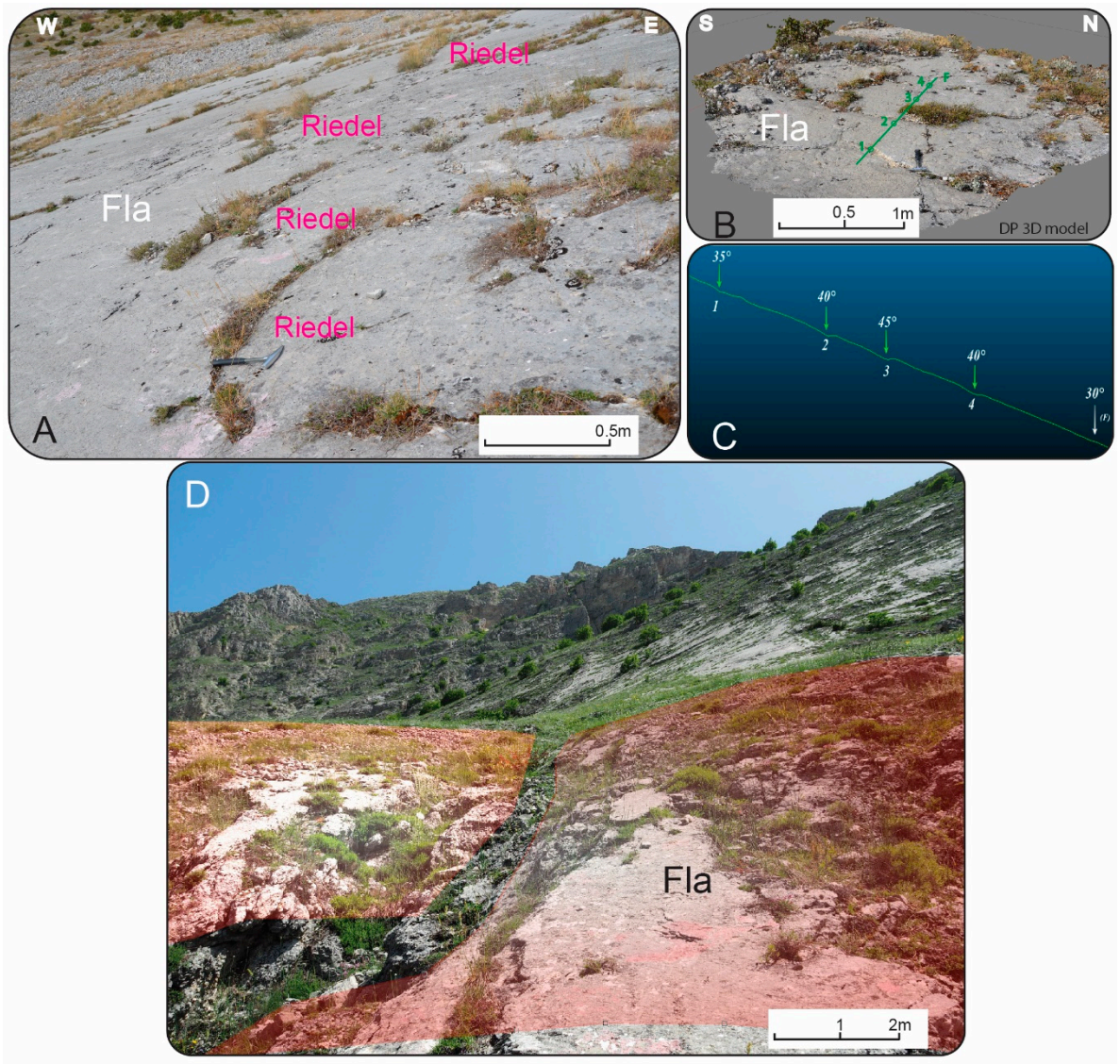

Figure 9. (**A**) Riedel shears on the main fault plane. (**B**) 3D reconstruction using DP. (**C**) The profile extracted from the 3D DP model shows the dip of the Riedel surfaces increases approximately 15 degrees in relation to the main fault surface. (**D**) Main sliding surface enveloping low-angle intersecting fault planes (red shadows) and forming metric to decametric sigmoidal structures.

Using the approach proposed by Byerlee [49], the average friction angle of the Fla was calculated to be approximately 35°. The rock strata (bedding planes) show a variable orientation, with a generalised NW-SE orientation, and ranging from vertical to NE dipping. Along the main SW dipping faults, the rock strata appear dragged towards the SW. The bedding plane measurements have been undertaken using both field measurements and data extracted from GIS thematic maps (Figure 10).

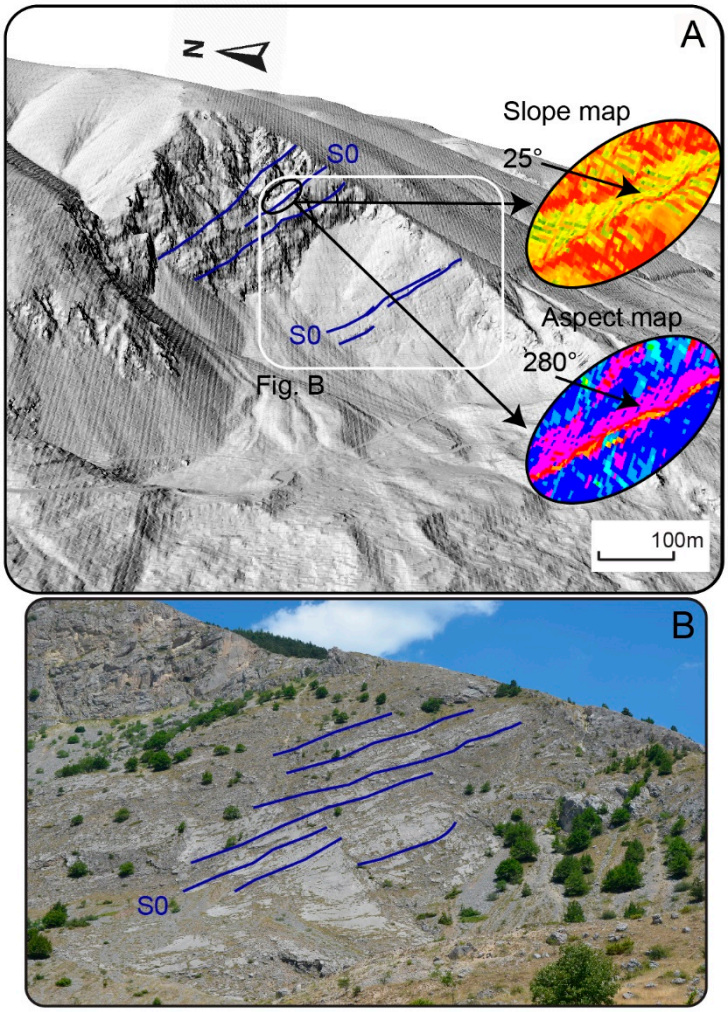

Figure 10. (**A**) Bedding planes (S0) highlighted on the Hillshade map and example of the extraction of dip (25°) and dip direction (280°) from Slope and Aspect maps. (**B**) Photograph of the landslide scar with highlighted cut-off lines (intersection between S0 and Fla).

Figure 10A shows the GIS approach, highlighting the identified bedding planes in the Hillshade map and the extraction of dip and dip direction from the slope and aspect maps, respectively. Figure 10B shows the landslide scar characterized by the intersection (cut-off lines) between the bedding and Fla. To validate this procedure and to better characterize the bedding attitude, a similar analysis has been carried in CloudCompare, where the LiDAR-extracted point cloud was analyzed using the software "compass" plug-in. The range in the value of the bedding measurements related to the landslide scar is reported in Table 3.

Table 3. Main discontinuity sets and their characteristics.

Set	Dip (°)	Dip Direction (°)	Spacing (m)	Persistence (m)	Infilling	Roughness	Weathering	UCS (MPa)
S0	7–45	240–280	5–10	20	Soft	Rough	High	40–60
J1	80	230	6–14	20	Soft	Smooth	High	50–70
J2	75	140	1–12	20	Soft	Smooth	High	50–70

The structural setting of the landslide area is summarized in the geological and geomorphological cross-section (Figure 11) which highlights the geometry of the fault zone along the Mt. Genzana and Mt. Rava slope.

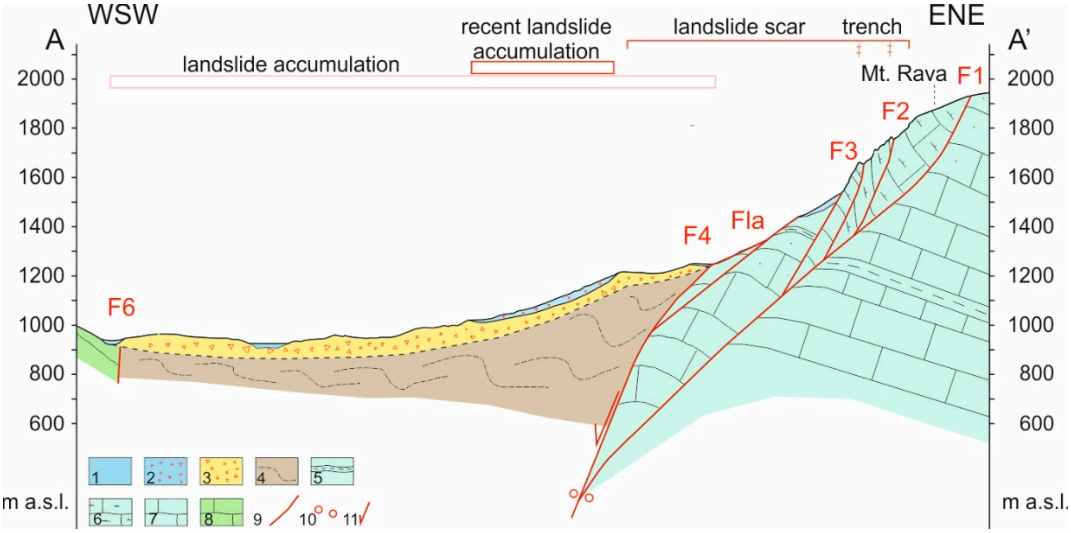

Figure 11. Geological cross-section of the Scanno landslide area showing the reconstructed geometry of the DMG fault zone, characterized by two main faults (F1, F4) enveloping low (Fla) and high-angle fault planes. The trace of section is localized in Figure 7. Legend: (1) fluvial deposits and talus slope deposits; (2) recent landslide deposits deposits; (3) Scanno landslide deposits; (4) Neogene pelitic-arenaceous siliciclastic rocks; (5) clay-marly levels (Jurassic-Cretaceous); (6) marly-limestone (Cretaceous); (7) limestone and marly-limestone (Jurassic-Cretaceous); (8) limestone (Jurassic-Miocene). (9) fault; (10) strike-slip fault movement; (11) normal fault movement.

4.2. Geomorphological Features

The geomorphological features in the landslide area are mainly characterized by structural and gravity-induced landforms (Figure 7).

The eastern flank of the valley features a system of fault-related scarps. Some of them are erosional features exhuming a buried fault plane (i.e., fault line scarps), other are interpreted to be directly related to recent (late Pleistocene-Holocene) movements of the fault (i.e., fault scarp in the Frattura area). Other structural scarps characterize the Frattura area, corresponding to the cemented layers of breccia deposits. In addition, minor hanging valleys strike across the slope along the main fault.

Figure 12 shows a detailed geomorphological map of the landslide scar area. The gravity-induced landforms form the principal features of the Scanno landslide scar and accumulation area, with different generations of talus slopes and cones and recent landslides overlaying the main landslide. The scarp of the main landslide shows an irregular arcuate shape (Figures 6A and 12 and Figure 13A). It features a rugged step-like upper part which is deeply weathered and a smoothed concave lower part (Figure 13B,C). The upper part is characterized by NW-SE trenches developed along the main and secondary faults (F2 and F3), which continue toward the NW, beyond the landslide scar (Figures 12 and 13D). The scarp has been affected by minor rockfalls and by debris falls which also extend beyond

the main landslide. This post-failure activity has resulted in talus slopes and talus cones at the junction between the upper and the lower parts of the scarp (Figures 12 and 13B). These talus deposits partially cover a smoothed rock surface observed in the southern part of the scarp (Figures 10, 12 and 13C), which corresponds to one of the main sliding surfaces of the landslide.

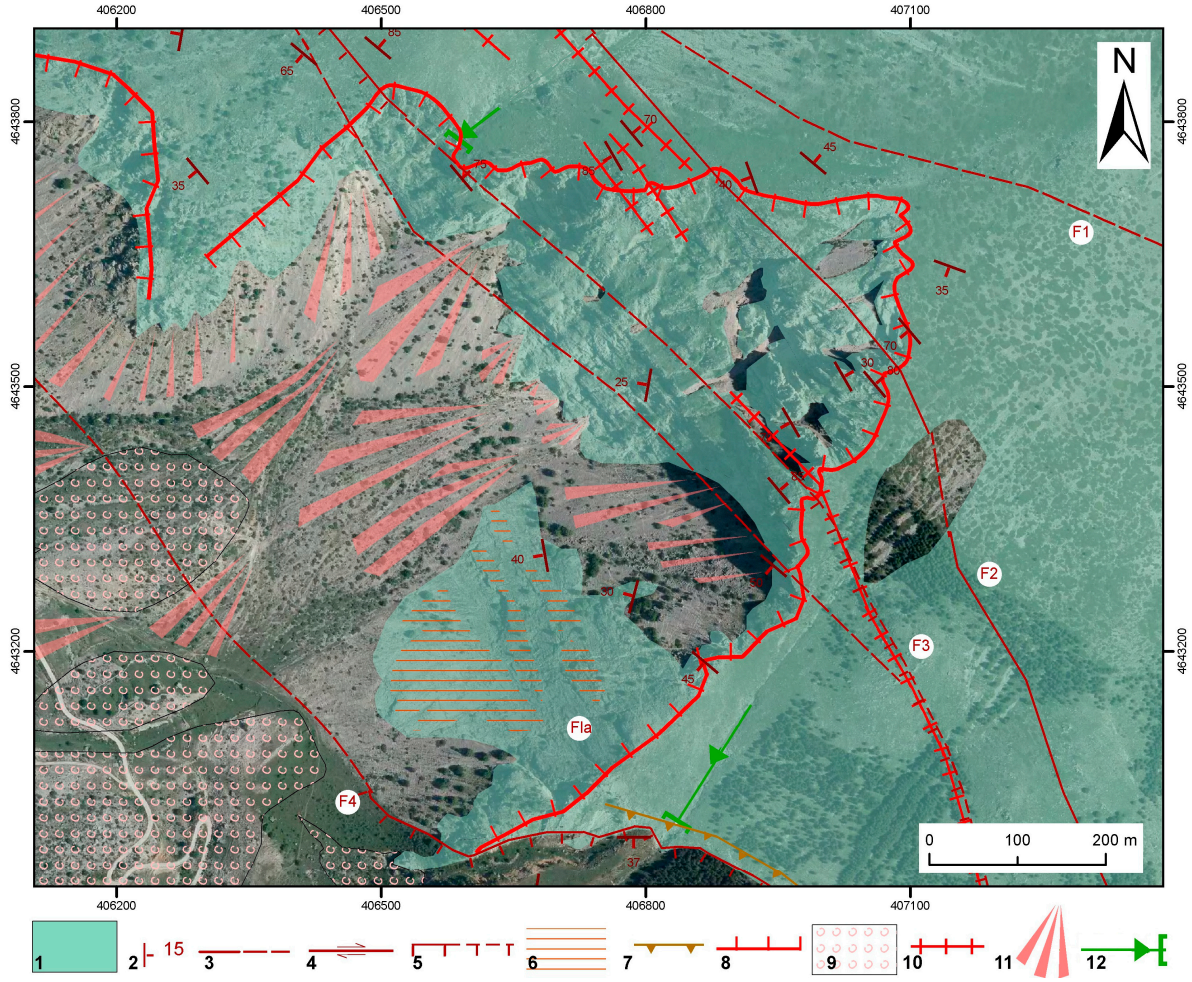

Figure 12. Geomorphological map of the landslide scar area. Legend: Bedrock: (1) Jurassic-Paleogene limestone and marly-limestone. Tectonics: (2) strata attitude (number is the dip angle); (3) fault (dashed if uncertain or buried); (4) strike-slip fault; (5) normal fault (dashed if uncertain or buried); (6) fault surface (Fla). Geomorphology: (7) fault scarp; (8) landslide scarp; (9) landslide; (10) trench; (11) talus cones; (12) hanging valley.

Different generations of talus cones and mixed talus/debris cones cover the sliding surface (lower part of the landslide scar). Small accumulations of landslide deposits are preserved within the concave scar of the main landslide as a result of weathering of the upper part of the scarp. The landslide accumulation is gently sloping and rugged (Figure 13E,F) with longitudinal and transversal morphological features. The bottom of the valley is characterized by alluvial fans and an alluvial plain covering the landslide deposits. The upper part of the main landslide scarp and the slope surrounding it (specifically in the northern part), is affected by a major trench located parallel to the slope strike and along minor faults and major joints within the DMG fault zone. These features outline possible locations for further instability in the Mount Genzana slope along the northern side of the present landslide scarp.

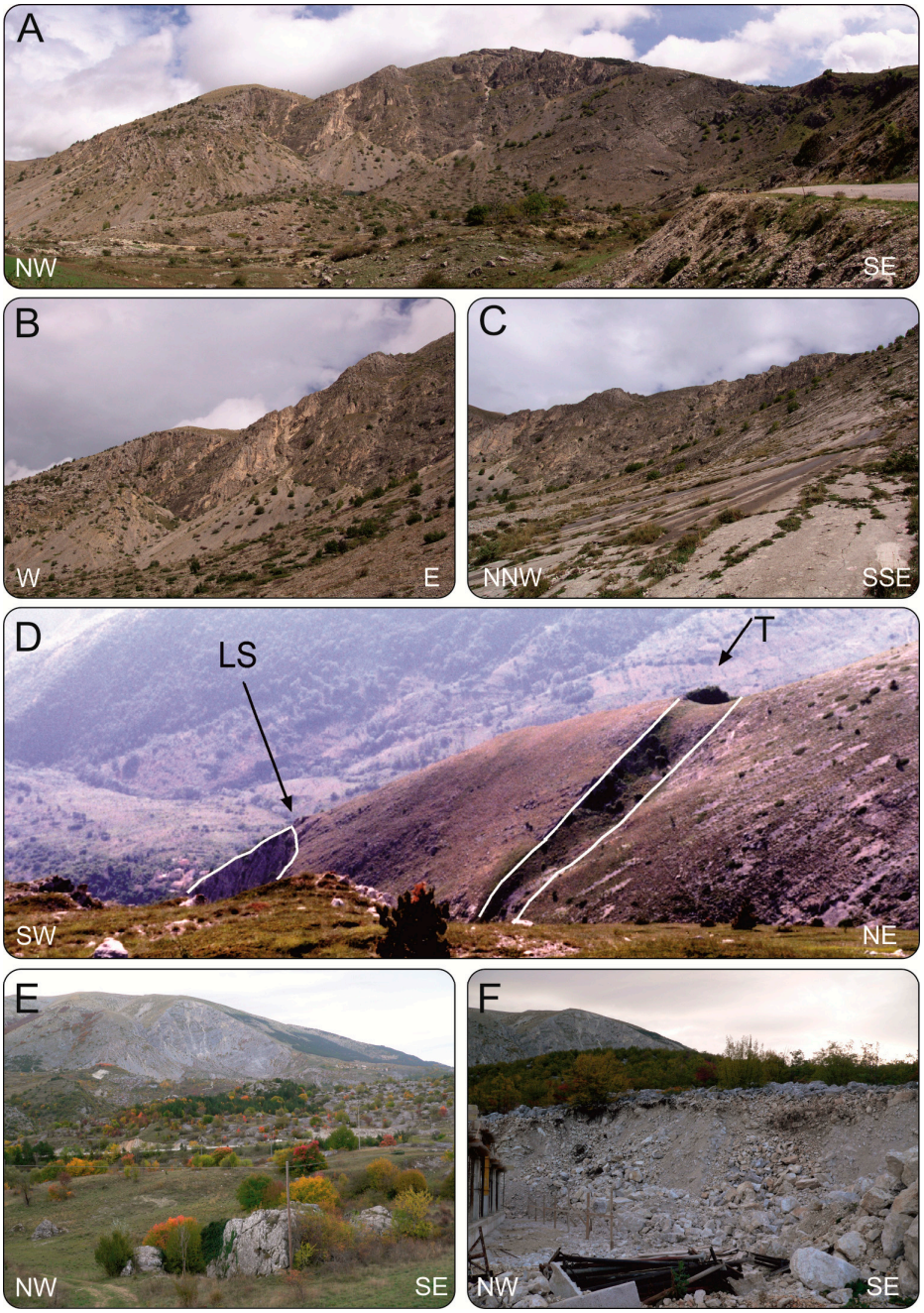

Figure 13. Main geomorphological features of the Scanno landslide. (**A**) Landslide scar; (**B**) weathering of the back scarp and talus cone formation; (**C**) sliding surface; (**D**) large trench (T) in the upper part of the slope, above the landslide scarp edge (LS); (**E**) accumulation area; (**F**) landslide deposits.

4.3. Generation of Pre- and Post-Failure Models

In order to approximate the volume of the Scanno landslide, the authors have attempted to recreate the pre-failure model of the area (Figure 14A). The topography of the pre-failure slope was created in two main steps: (i) the contour lines representing the landslide scar and accumulation area (red polygon in Figure 14B) were removed; ii) the contour lines of the surrounding slope faces were projected into the landslide area to recreate the slope pre-failure. Step (ii) was performed using an iterative approach which allowed to find an agreement between the reconstructed topography and the expected volume of landslide (and accumulated materials). Figure 14A,B shows the result of this process, highlighting the difference between the pre- and post-failure 3D models.

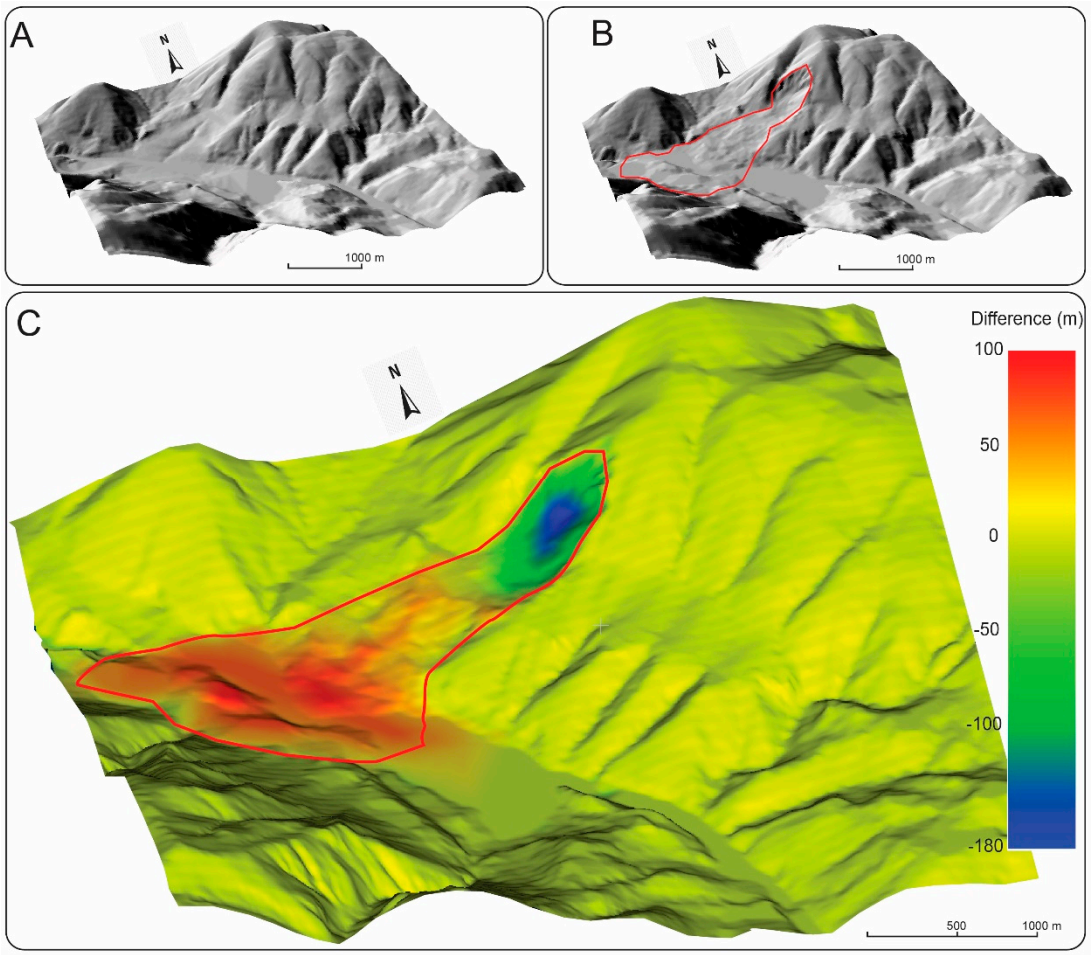

Figure 14. (**A**) Pre-failure model of the landslide. (**B**) Post-failure model of the landslide. (**C**) Comparison of the two models carried out in CloudCompare [44].

From these models, two-point clouds were extracted and compared in the software CloudCompare [44] (Figure 14C). The volume calculated through this comparison was ca 100×10^6 m^3.

4.4. Geomechanical Model and Back-Analysis

The geomechanical analysis was conducted by integrating literature data, conventional geomechanical survey data and DP. Geomechanical surveys were carried out in accessible outcrops (East flank) of the landslide area (Figure 5A), while DP was used to create the 3D model of the inaccessible W-NW flank of the back scarp (Figure 5A,B). The mean square error obtained during the creation of the 3D model was approximately 0.3 m, with the use of LiDAR for determining ground control points. However, the authors deem this error acceptable in consideration of the extent of the outcrop, ca 200 m high × 200 m wide. The integration of geomechanical and DP data highlighted two main discontinuity sets, J1 and J2, NW and NE striking, respectively. Table 3 shows the main characteristics of the discontinuity sets, while Figure 15 shows the DP model with the main joint sets, J1 and J2, highlighted.

Intact rock mass properties were obtained from Della Seta et al. [5] and can be summarized as follows: Unit Weight = 25 kN/m^3; Friction = 57°; Cohesion = 13.6 MPa; Tensile strength = 9.2 MPa; Bulk modulus = 19,000 MPa and Shear modulus = 11,000 MPa.

Data from conventional geomechanical and DP surveys were used to develop the kinematic model of the landslide. Figure 16A shows the 3D model of the landslide and the stereonet obtained from the discontinuity measurements. The low-angle fault, Fla, likely formed the basal failure surface (red area).

Joint sets J1 and J2 acted as a lateral release surface on the NW flank (blue area) with the back scarp (orange area) being characterized by the interaction of J1 and J2 and fault F2–F3. Figure 16B–D show three examples of the observed rock mass, GSI, defined using field (Figure 16B) and remote sensing data (Figure 16C,D). The GSI values vary in relation to the structural location within the landslide scar, being very low in fault cataclastic damage zone (Figure 16B) and higher in the area affected by the intersection of discontinuity sets (Figure 16C,D).

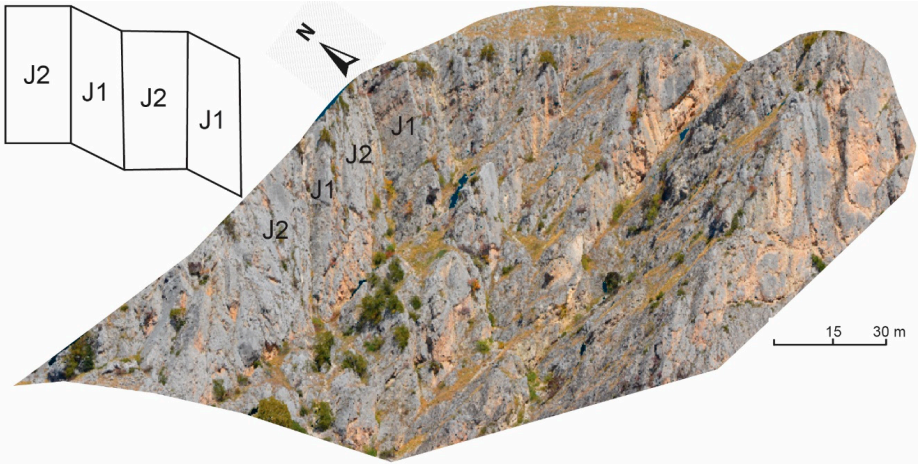

Figure 15. Discontinuity sets J1 and J2 indicated on the DP model.

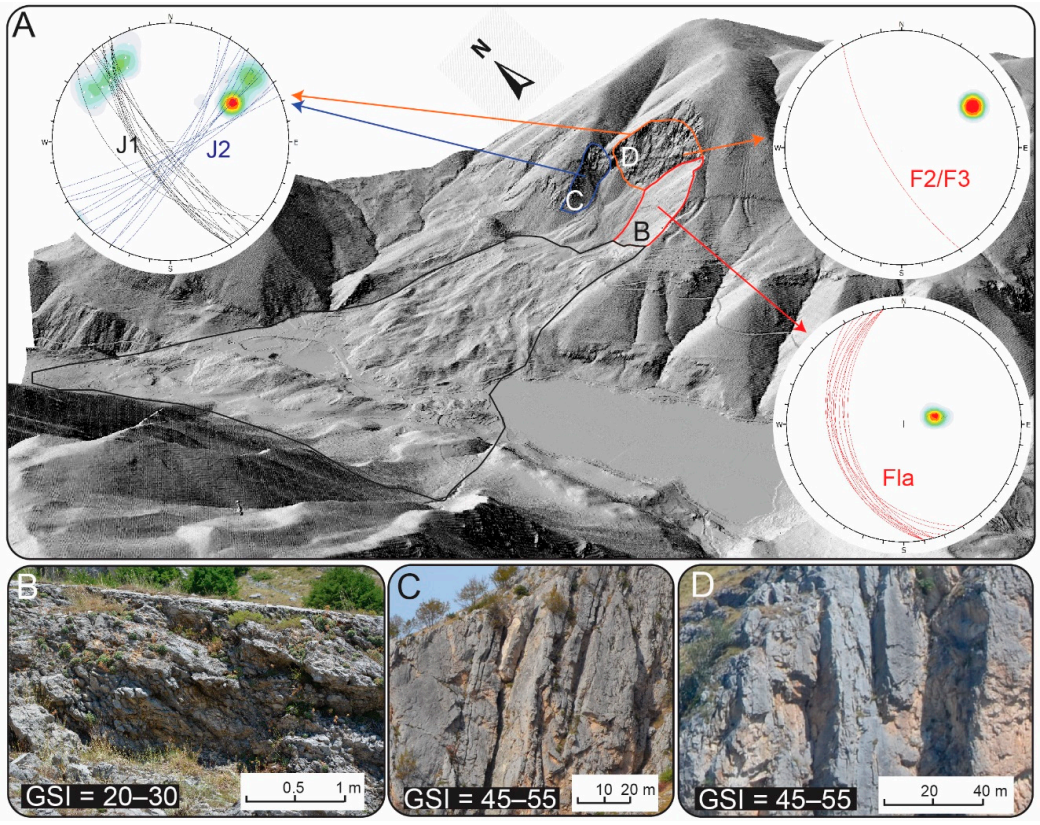

Figure 16. (**A**) 3D model of the landslide and stereonets obtained from the mean discontinuity measurements. The red line represents Fla failure surface, the blue line is the lateral release surface, the orange line is the back scarp and black line includes the landslide deposit, (**B**) Rock mass conditions in vicinity of cataclastic zone, and (**C**), (**D**) Rock mass conditions in areas characterized by intersecting joint sets.

The GSI values were used in RocData v. 5 [45] to constrain the residual rock mass friction angle. It has been found that when the GSI is 20–30, the rock mass friction angle is approximately 35° and increases up to 40° when the GSI is 40–50.

The kinematic/geomechanical model was used to run limit equilibrium analyses in static and dynamic conditions, with Fla used as failure surface and F2–F3 as back-scarps. The initial static simulation carried out using RocPlane provided an initial parametric sensitivity study of friction angle and cohesion (Figure 17A). These simulations showed a variation of Factor of Safety ranging from 1.5 to 1.9 (Figure 17A–B) and demonstrated the predominant role of friction on stability (Figure 17A). A further analysis was run including a seismic coefficient ranging from 0.250 g to 0.275 g, assuming the same range of friction angle used in the static analysis. The value of cohesion was shown to have only a minor influence in the variation of the Factor of Safety, and was therefore conservatively set to 0 MPa. When the analysis included the seismic coefficient, the Factor of Safety ranged from stable (1.14 in the case of low seismic coefficient and high friction angle values) to an unstable condition (below 1 in the case of high seismic coefficient and low friction angle values) (Figure 17C).

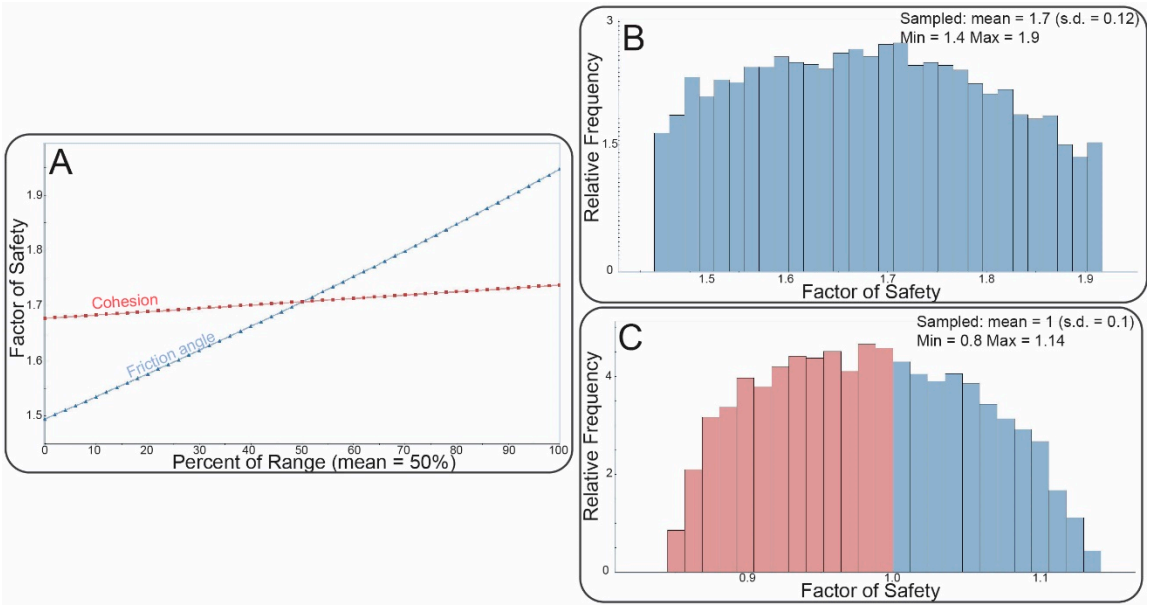

Figure 17. Limit equilibrium analysis. (**A**) Sensitivity analysis of cohesion and friction angle showing predominant control of friction angle on the variation of the Factor of Safety. (**B**) Possible variation in the Factor of Safety under static conditions. (**C**) Possible variation in the Factor of Safety assuming dynamic conditions.

With the goal of constraining the results of RocPlane limit equilibrium analysis and using the observed 3D geometry of the slope, a further analysis was performed with Slide3. The pre-failure model shown in Figure 14A was used to create the geometry of the slope while the landslide scar (Figure 16), formed by Fla and discontinuity sets, was used to generate the failure surface. According to the results of the RocPlane simulation, the cohesion was selected and the results assuming different values of friction angle and seismic coefficient investigated. The 3D Slide3 model analysed is shown in Figure 18A. Figure 18B illustrates example results, in terms of base normal stress, and a graph presenting the calculated Factor of Safety under static and dynamic conditions for a range of friction angles from 30° to 40° (in agreement with the RocPlane analysis and the residual friction angle obtained from the RocData analysis). In the static condition the Factor of Safety (FS) varies from ca 1.3 to 1.8, while under dynamic conditions the FS ranged from stable (1.2 in the case of low seismic coefficient and high friction angle values) to an unstable condition (below 1 in the case of high seismic coefficient and low friction angle values) (Figure 18B).

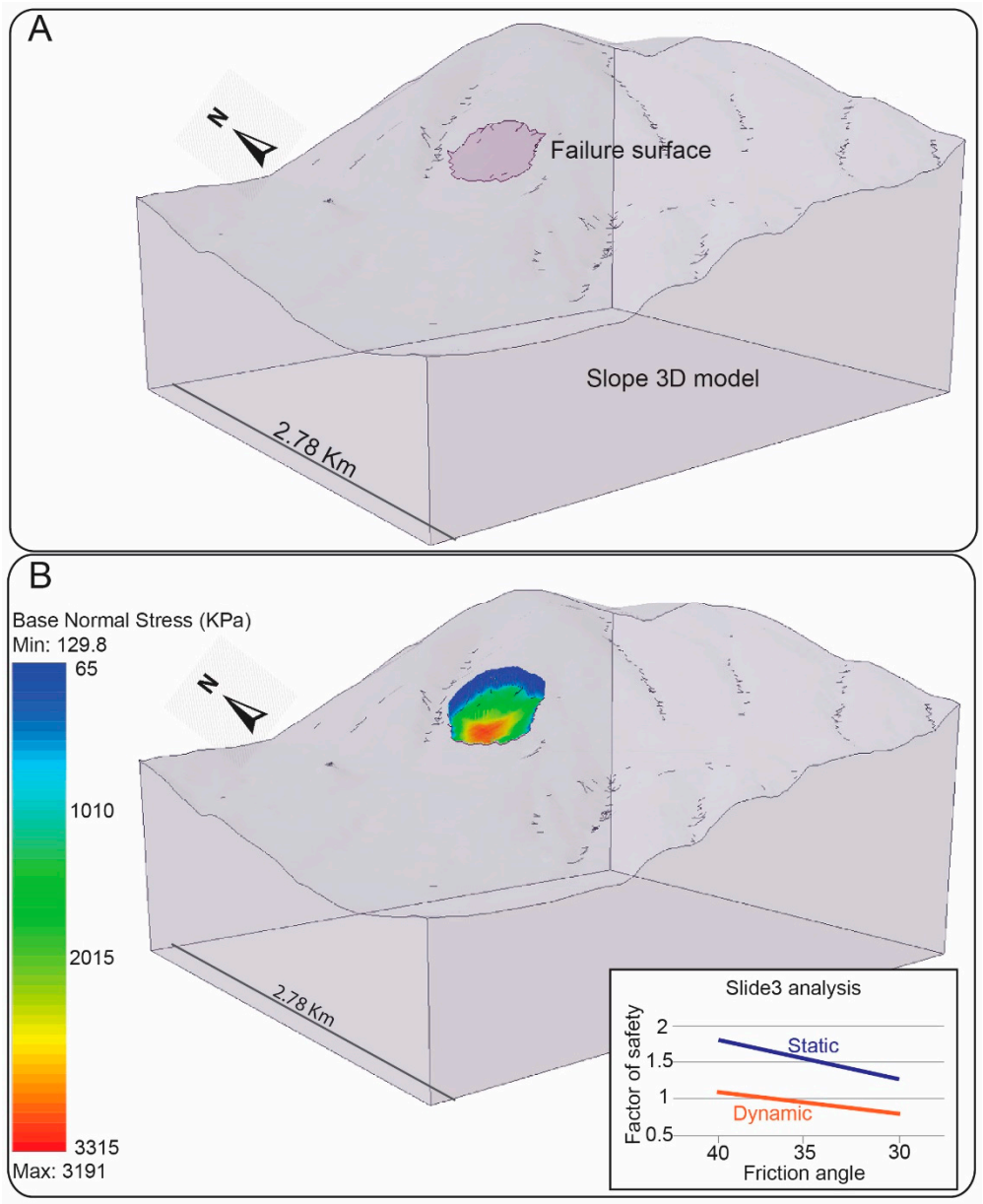

Figure 18. (**A**) Slide3 3D model created using pre- and post- failure 3D models. (**B**) Example of results (in terms of base normal stress) obtained from Slide3 analysis and a graph showing the resulting FS for static and dynamic conditions using a range of friction angles from 30° to 40°.

5. Discussion

The integration of different methods of survey and analysis, such as geology, geomorphology and geomechanics, can play a key role in the analysis of landslides and paleo-landslides. In this research, the geological and geomorphological analyses provided a basis to improve the geological model of the Scanno area with the aim of showing the kinematic constraints of the Scanno landslide. The surveys aided in the classification of a geological-faulting model based on the identification of the Fla fault, forming the Scanno landslide failure surface. The Fla fault is part of the complex DMG fault zone, which is characterized by the interaction of low- and high-angle faults. The DMG fault zone can therefore be interpreted according to an extensional duplex [48] related to the interaction of dip-slip and strike-slip kinematics. The interaction of low- and high-angle faults provides the geometry required for the landslide failure, with the Fla acting as the basal failure surface and F2/F3 as back-scarps. Figure 19 shows the 2D structural setting of the DMG fault zone pre-landslide (Figure 19A), the failure conditions

(Figure 19B) and the post-failure setting (Figure 19C). This interpretation differs significantly from Bianchi-Fasani et al. [4] and Della Seta et al. [5] who described the Scanno landslide as a rock avalanche that failed along bedding planes.

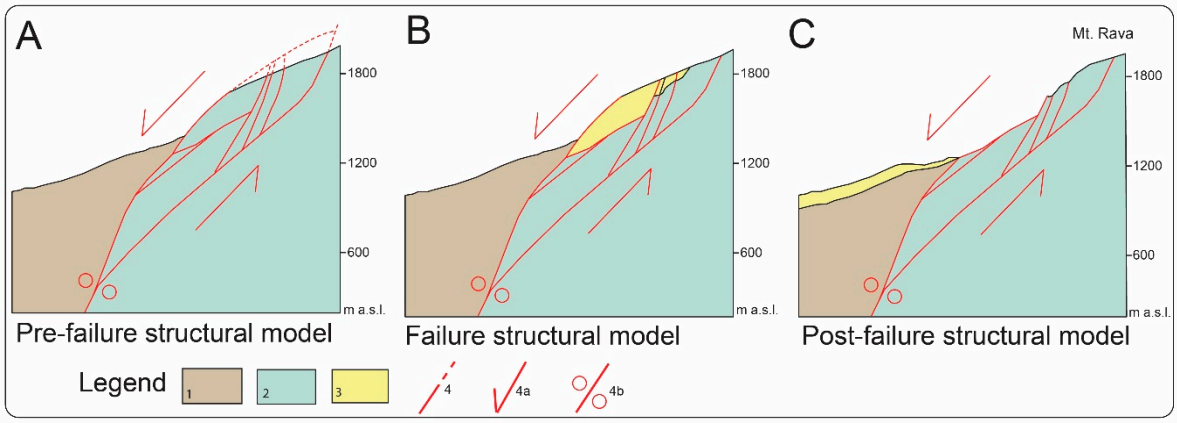

Figure 19. Pre- and post-failure structural models of the Scanno landslide, showing the structural setting of the DMG fault zone composed of low- and high-angle fault planes, typical of a duplex geometry, controlled by dip-slip and strike-slip kinematics. The low-angle faults represent the main slip planes of rock avalanches: (**A**) Pre-landslide model. (**B**) Failure conditions. (**C**) Post-failure model. Legend: Bedrock: (1) Neogene pelitic-arenaceous siliciclastic rocks; (2) Jurassic-Paleogene limestone and marly-limestone. Geomorphology: (3) Landslide (pre- and post-failure). Tectonics: (4) Fault (dashed when inferred); (4a) Normal fault; (4b) Strike-slip fault.

By integrating the new data set with the data obtained by DP and LiDAR, the authors have created a geomechanical model of the landslide that highlights the importance of a multi-disciplinary evaluation of large rock avalanches. A similar approach, integrating remote sensing and structural data was also shown in the study of rocky cliffs by Frodella et al. [50], Tysiac et al. [12], Francioni et al. [16]. A critical review showing the importance of structural geology in understanding landslide failure mechanisms was presented by Stead and Wolter [51]. In this research, LiDAR data was essential for creation of a 3D model of the slope and improving the understanding of the detrimental effects of structural features (bedding planes and main faults) on landslide stability. The importance of using LiDAR data in the acquisition and monitoring of geological processes has been discussed by numerous authors including Gorsevski et al. [52], Kamps et al. [53] and Ortuno et al. [54]. When dealing with steep rocky slopes, geomechanical surveys can only be carried out in accessible areas and LiDAR data are not always appropriate due to limitations associated with the nadir point of view of the aircraft and the resolution of the extracted digital elevation model (1m in this case). For this reason, the use of DP played an important role, aiding in the definition and identification of the characteristics of the two main joint sets. The approach used was based on hand-held DP technique which, according to Francioni et al., [55], represents one of the most cost-effective methods of using DP. However, due to the extensive area of the site and the distance from the slope, the use of more innovative UAV systems could improve the data and results obtained, as shown in recent research by Rossi [18], Giordan et al. [56] Mancini et al. [57], Vanneschi et al. [58] and Liu et al. [59].

The use of GIS techniques provided a platform to manage the data obtained from the aforementioned surveys and was crucial in the development of thematic and pre- and post-failure 3D models of the landslides. Using this approach, it was possible to calculate the volume of the landslide. This was in agreement with Scarascia Mugnozza et al. [38] (volume of 96×10^6 m^3) which was similar, although, slightly larger than the 86×10^6 m^3 obtained by Nicoletti et al. [3].

The geomechanical model was also used as a basis to perform a back-analysis of the landslide. The friction angle of the fault, Fla, was defined using the approach proposed by Byerlee [49] while the rock mass residual friction angle was estimated using GSI and RocLab. A sensitivity analysis was

performed to understand the role of friction angle and cohesion on the Factor of Safety. The analysis showed the controlling role of the friction angle in the calculation of the Factor of Safety. Furthermore, two further analyses were carried out under both static conditions and dynamic conditions, using the limit equilibrium software RocPlane and Slide3. This analysis revealed the increased probability of failure when the seismic coefficient is considered, suggesting a possible seismic trigger for the Scanno landslide. This agrees with Scarascia Mugnozza et al. [38] and Colarossi-Mancini [60], who hypothesized the seismic nature of the landslide, without, however, supporting such a hypothesis with back-analyses of the instability. It should be noted that the limit equilibrium analyses presented herein have been carried out to understand the role of seismicity and represent a simplified kinematic model of the landslide. However, the aforementioned DMG fault zone represents a very complex fault zone, characterized by the interaction of low- and high-angle faults and two main joint sets. In proximity of the fault, cataclastic fault damage zones result in very low GSI values, decreasing the rock mass residual friction angle. In light of the presented evidence, the structural setting of the area, characterized by a wide fault zone with high- and low-angle faults and the occurrence of a high magnitude seismic event, can be considered the two main causes of the rock mass failures. Other factors, such as rainfall and extreme weather conditions, might also be contributory causes of the failure. However, the principal role played by the structural condition of the landslide area is confirmed by the fact that the Scanno landslide, located at the centre of the DMG fault zone, is a unique case study in the Central Apennines; being one of the largest rock avalanches recognized in the area having generated the biggest dammed lake in Central Italy. The importance and peculiarity of such an event is also highlighted by the stability of the landslide dam c. 12,000 years after its formation. This has been studied by Bianchi-Fasani et al. [4] and is related to the high volume of debris generated by the failure and the small dam height–length ratio.

6. Conclusions

The Scanno landslide is located in the Tasso Stream and Sagittario River drainage basin, downstream from the Scanno Lake. The landslide has been defined as a large rock avalanche which occurred at the end of Late Pleistocene on the western slope of the Mt. Genzana ridge, Central Apennines (Italy). The landslide dammed the Sagittario River, forming the Scanno Lake, one of the most famous landslide-dammed lakes in Italy.

In this research, the authors performed an integrated investigation incorporating geological, geomechanical and geomorphological surveys, LiDAR analysis, digital photogrammetry, kinematic and limit equilibrium back-analyses. Our results provide new important contributions related to the geomechanical/structural model and improved understanding of the factors triggering the landslide. The main findings can be summarized as:

- The Scanno landslide area is characterized by a wide failure scar area, which is interpreted as an exposed low-angle fault.
- The scar is controlled by the low-angle normal fault planes associated with Difesa-Monte Genzana-Vallone delle Masserie (DMG) fault zone; high-angle faults (SW dipping, F2–F3) and joints (two sets dipping toward SW and SE) which represent the backscarp surfaces and lateral release surfaces of the Scanno landslide.
- Bedding planes form intersection (cut-off) lines along the landslide scar/fault plane.
- The creation of pre- and post-failure 3D models of the landslide provided the basis for analysis that suggests the landslide morphometry involved a 2.7×10^6 m^2 surface area and a 100×10^6 m^3 estimated volume, similar or slightly higher than estimations from previous investigators.
- The limit equilibrium back-analyses showed a Factor of Safety ranging from 1.2 to 2.0 when static conditions are assumed. When dynamic conditions are considered (PGA 0.250–0.275 according to the Italian seismic hazard map, Gruppo di Lavoro MPS, 2004), the Factor of Safety ranged from stable (1.1 in the case of a low seismic coefficient and high friction angle values) to an unstable condition

(below 1 in the case of a high seismic coefficient and low friction angle values). This strongly suggests that the landslide was probably triggered by a seismic event consistent with the present tectonic regime related to active extensional tectonics involving the axial zone of Apennine Mountain Ridge (most likely related to magnitude 4.5–6.5 seismic events within 10 km of the Scanno area), in agreement with data available from the Italian seismic database and hazard map.

Author Contributions: For research articles with several authors, a short paragraph specifying their individual contributions must be provided. The following statements should be used "conceptualization, M.F., F.C., T.P., N.S., D.S. and E.M..; methodology, M.F., F.C., J.C., T.P. and E.M.; software, M.F., M.E. and A.D.N.; validation, J.C., D.S., M.E. and N.S.; formal analysis, M.F., A.D.N. and T.P; investigation, M.F., A.D.N., F.C. and T.P.; resources, F.C., J.C., E.M. and N.S.; data curation, M.F. and T.P.; writing—original draft preparation, M.F. and T.P.; writing—review and editing, F.C., D.S., J.C., M.E., E.M. and N.S.; visualization, M.F., T.P. and M.E.; supervision, F.C., E.M., D.S. and N.S.; project administration, M.F., F.C., N.S. and E.M.; funding acquisition, F.C. and E.M.", please turn to the CRediT taxonomy for the term explanation. Authorship must be limited to those who have contributed substantially to the work reported.

Funding: This research received no external funding.

Acknowledgments: The authors would like to express their gratitude to the reviewers who provided important and constructive suggestions for improving the quality of the paper.

Conflicts of Interest: The authors declare no conflict of interest.

References

1. Dussauge, C.; Grasso, J.R.; Helmstetter, A. Statistical analysis of rockfall volume distributions: Implications for rockfall dynamics. *J. Geophys. Res.* **2003**, *108*, 2286. [CrossRef]
2. Marinelli, O. *Atlante dei Tipi Geografici*; Istituto Geografico Militare: Firenze, Italy, 1922; p. 904.
3. Nicoletti, G.; Parise, P.G.; Miccadei, E. The Scanno Rock Avalanche (Abrezzi, South Central Italy). *Boll. Soc. Geol. Ital.* **1993**, *112*, 523–535.
4. Bianchi-Fasani, G.; Esposito, C.; Petitta, M.; Scarascia Mugnozza, G.; Barbieri, M.; Cardarelli, E.; Cercato, M.; Di Filippo, G. The importance of geological models in understanding and predicting the life span of rockslide dams: The case of Scanno Lake, Central Italy. Natural and artificial rockslide dams. *Lect. Notes Earth Sci.* **2011**, *133*, 323–345.
5. Della Seta, M.; Esposito, C.; Marmoni, G.M.; Martino, S.; Scarascia Mugnozza, G.; Troiani, F. Morpho-structural evolution of the valley-slope systems and related implications on slope-scale gravitational processes: New results from the Mt. Genzana case history (Central Apennines, Italy). *Geomorphology* **2017**, *289*, 60–77. [CrossRef]
6. Agliardi, F.; Crosta, G.; Zanchi, A. Structural constraints on deep-seated slope deformation kinematics. *Eng. Geol.* **2001**, *59*, 83–102. [CrossRef]
7. Gigli, G.; Morelli, S.; Fornera, S.; Casagli, N. Terrestrial laser scanner and geomechanical surveys for the rapid evaluation of rock fall susceptibility scenarios. *Landslides* **2014**, *11*, 1–14. [CrossRef]
8. Martino, S.; Mazzanti, P. Integrating geomechanical surveys and remote sensing for sea cliff slope stability analysis: The Mt. Pucci case study (Italy). *Nat. Hazards Earth Syst. Sci.* **2014**, *14*, 831–848. [CrossRef]
9. Li, X.; Chen, J.; Zhu, H. A new method for automated discontinuity trace mapping on rock mass 3D surface model. *Comput. Geosci.* **2016**, *89*, 118–131. [CrossRef]
10. Tuncay, E. Assessments on slope instabilities triggered by engineering excavations near a small settlement (Turkey). *J. Mt. Sci.-Engl.* **2018**, *15*, 114–129. [CrossRef]
11. Lato, M.J.; Gauthier, D.; Hutchinson, D.J. Rock slopes asset management: Selecting the optimal three-dimensional remote sensing technology. *Transp. Res. Rec.* **2015**, *2510*, 7–14. [CrossRef]
12. Tysiac, P.; Wojtowicz, A.; Szulwic, J. Coastal cliffs monitoring and prediction of displacements using Terrestrial laser scanning. In Proceedings of the Baltic Geodetic Congress (BGC Geomatics), Gdansk, Poland, 2–4 June 2016. [CrossRef]
13. Ossowski, R.; Tysiac, P. A New approach of coastal cliff monitoring using mobile laser scanning. *Pol. Marit. Res.* **2018**, *25*, 140–147. [CrossRef]
14. Riquelme, A.; Tomás, R.; Cano, M.; Pastor, J.L.; Abellán, A. Automatic mapping of discontinuity persistence on rock masses using 3D point clouds. *Landslides* **2018**, *51*, 3005–3028. [CrossRef]

15. Ferrero, A.M.; Migliazza, M.; Roncella, R.; Segalini, A. Rock cliffs hazard analysis based on remote geostructural surveys: The Campione del Garda case study (Lake Garda, Northern Italy). *Geomorphology* **2011**, *4*, 457–471. [CrossRef]
16. Francioni, M.; Coggan, J.; Eyre, M.; Stead, D. A combined field/remote sensing approach for characterizing landslide risk in coastal areas. *Int. J. Appl. Earth Obs. Geoinf.* **2018**, *67*, 79–95. [CrossRef]
17. Francioni, M.; Stead, D.; Sciarra, N.; Calamita, F. A new approach for defining Slope Mass Rating in heterogeneous sedimentary rocks using a combined remote sensing GIS approach. *Bull. Eng. Geol. Environ.* **2018**, 1–22. [CrossRef]
18. Rossi, G.; Tanteri, L.; Tofani, V.; Vannocci, P.; Moretti, S.; Casagli, N. Multitemporal UAV surveys for landslide mapping and characterization. *Landslides* **2018**, *15*, 1045–1052. [CrossRef]
19. Calista, M.; Miccadei, E.; Piacentini, T.; Sciarra, N. Morphostructural, meteorological and seismic factors controlling landslides in weak rocks: The case studies of Castelnuovo and Ponzano (North East Abruzzo, Central Italy). *Geosciences* **2019**, *9*, 122. [CrossRef]
20. Riquelme, A.J.; Tomás, R.; Abellán, A. Characterization of rock slopes through slope mass rating using 3D point clouds. *Int. J. Rock Mech. Min. Sci.* **2016**, *84*, 165–176. [CrossRef]
21. Zhao, C.; Lu, Z. Remote sensing of landslides—A review. *Remote Sens.* **2018**, *10*, 279. [CrossRef]
22. Kasai, M.; Ikeda, M.; Asahina, T.; Fujisawa, K. LiDAR-derived DEM evaluation of deep-seated landslides in a steep and rocky region of Japan. *Geomorphology* **2009**, *113*, 57–69. [CrossRef]
23. Abdulwahid, W.M.; Pradhan, B. Landslide vulnerability and risk assessment for multi-hazard scenarios using airborne laser scanning data (LiDAR). *Landslide* **2017**, *14*, 1057–1076. [CrossRef]
24. Brideau, M.A.; Pedrazzini, A.; Stead, D.; Froese, C.; Jaboyedoff, M.; van Zeyl, D. Three-dimensional slope stability analysis of South Peak, Crowsnest Pass, Alberta, Canada. *Landslide* **2011**, *8*, 139–158. [CrossRef]
25. Francioni, M.; Stead, D.; Clague, J.J.; Westin, A. Identification and analysis of large paleo-landslides at Mount Burnaby, British Columbia. *Environ. Eng. Geosci.* **2018**, *24*, 221–235. [CrossRef]
26. Jaboyedoff, M.; Oppikofer, T.; Abellan, A.; Derron, M.E.; Loye, A.; Metzger, R.; Pedrazzini, A. Use of LIDAR in landslide investigations: A review. *Nat. Hazards* **2012**, *61*, 5–28. [CrossRef]
27. INGV. *Mappe Interattive Della Pericolosità Sismica D'italia*; Istituto Nazionale di Geofisica e Vulcanologia: Naples, Italy, 2004; Available online: http://esse1-gis.mi.ingv.it/ (accessed on 10 January 2019).
28. D'Agostino, N.; Jackson, J.A.; Dramis, F.; Funiciello, R. Interactions between mantle upwelling, drainage evolution and active normal faulting: An example from the Central Apennines (Italy). *Geophys. J. Int.* **2001**, *147*, 475–497. [CrossRef]
29. Miccadei, E.; Berti, C.; Calista, M.; Esposito, G.; Mancinelli, V.; Piacentini, T. Morphotectonics of the Tasso Stream—Sagittario River valley (Central Apennines, Italy). *J. Maps* **2019**, *15*, 257–268. [CrossRef]
30. Miccadei, E.; Mascioli, F.; Piacentini, T. Quaternary geomorphological evolution of the Tremiti Islands (Puglia, Italy). *Quat. Int.* **2011**, *232*, 3–15. [CrossRef]
31. ISPRA. Carta Geologica D'Italia Alla Scala 1:50.000, Foglio 378 "Scanno". Servizio Geologico D'Italia 2014. Available online: http://www.isprambiente.gov.it/Media/carg/378_SCANNO/Foglio.html (accessed on 29 November 2018).
32. Beneo, E. Insegnamenti di una galleria a propositi della tettonica nella Valle del Sagittario. *Boll. R Uff. Geol. Ital.* **1938**, *63*, 1–10.
33. Miccadei, E. Geologia dell'area Alto Sagittario-Alto Sangro (Abruzzo, Appennino centrale). *Geol. Romana* **1993**, *29*, 463–481.
34. Corrado, S.; Miccadei, E.; Parotto, M.; Salvini, F. Evoluzione tettonica del settore di Montagna Grande (Appennino centrale): Il contributo di nuovi dati geometrici, cinematici e paleogeotermici. *B Soc. Geol. Ital.* **1996**, *115*, 325–338.
35. Agostini, S.; Calamita, F. Il ruolo dell'eredita strutturale nello sviluppo della catena appenninica: l'esempio della Montagna Grande e del Monte Genzana (Appennino Centrale Abruzzese). *Rend. Online Della Soc. Geol. Ital.* **2009**, *5*, 13–16.
36. Calamita, F.; Di Domenica, A.; Pace, P. Macro-and meso-scale structural criteria for identifying pre-thrusting normal faults within foreland fold-and-thrust belts: Insights from the Central-Northern Apennines (Italy). *Terra Nova* **2018**, *30*, 50–62. [CrossRef]
37. Miccadei, E.; Piacentini, T.; Dal Pozzo, A.; La Corte, M.; Sciarra, M. Morphotectonic map of the Aventino-Lower Sangro valley (Abruzzo, Italy), scale 1:50,000. *J. Maps* **2013**, *9*, 390–409. [CrossRef]

38. Scarascia Mugnozza, G.; Petitta, M.; Bianchi Fasani, G.; Esposito, C.; Barbieri, M.; Cardarelli, E. The importance of geological model to understand and predict the life span of rockslide dams: The Scanno lake case study, Central Italy. *Ital. J. Eng. Geol. Environ.* **2006**, *1*, 127–132.
39. Carmisciano, C.; Marchetti, M.; Florindo, F.; Muccini, F.; Cocchi, L. *Geophysical Surveys in the Scanno Lake*; Quaderni di Geofisica; Istituto Nazionale di Geofisica e Vulcanologia (INGV): Naples, Italy, 2004; p. 116, ISSN 1590-2595.
40. Sibson, H.R. Fault rocks and fault mechanisms. *J. Geol. Soc.* **1977**, *133*, 191–213. [CrossRef]
41. Birch, J.S. Using 3DM analyst mine mapping suite for rock face characterization. In *Laser and Photogrammetric Methods for Rock Face Characterization*; Kottenstette, J., Tonon, F., Eds.; ARMA: Overland Park, KS, USA, 2006; pp. 13–32.
42. Hoek, E.; Brown, E.T. Practical estimates of rock mass strength. *Int. J. Rock Mech. Min. Sci.* **1997**, *34*, 1165–1186. [CrossRef]
43. ESRI. ArcGIS Desktop (Version 10.6). Available online: https://www.esri.com/en-us/arcgis/about-arcgis/overview (accessed on 12 November 2018).
44. CloudCompare. CloudCompare (Version 2.9). Available online: http://www.cloudcompare.org (accessed on 12 November 2018).
45. RocScience. Available online: https://www.rocscience.com/ (accessed on 17 January 2019).
46. Gruppo di Lavoro MPS. *Redazione Della Mappa di Pericolosità Sismica Prevista Dall'Ordinanza PCM 3274 del 20 Marzo 2003, Rapporto Conclusivo Per Il Dipartimento Della Protezione Civile*; INGV: Milano-Roma, Italy, 2004.
47. Bazzurro, P.; Cornell, C.A. Disaggregation of seismic hazard. *Bull. Seismol. Soc. Am.* **1999**, *89*, 501–520.
48. Fossen, H. *Structural Geology*, 2nd ed.; Cambridge University Press: Cambridge, UK, 2016; p. 387.
49. Byerlee, J.D. Friction of rocks. *Pure Appl. Geophys.* **1978**, *116*, 615–626. [CrossRef]
50. Frodella, W.; Ciampalini, A.; Gigli, G.; Lombardi, L.; Raspini, F.; Nocentini, M.; Scardigli, C.; Casagli, N. Synergic use of satellite and ground based remote sensing methods for monitoring the San Leo rock cliff (Northern Italy). *Geomorphology* **2016**, *264*, 80–94. [CrossRef]
51. Stead, D.; Wolter, A. A critical review of rock slope failure mechanisms: The importance of structural geology. *J. Struct. Geol.* **2015**, *74*, 1–23. [CrossRef]
52. Gorsevski, P.V.; Brown, M.K.; Panter, K.; Onasch, C.M.; Simic, A.; Snyder, J. Landslide detection and susceptibility mapping using LiDAR and an artificial neural network approach: A case study in the Cuyahoga Valley National Park, Ohio. *Landslides* **2016**, *13*, 467–484. [CrossRef]
53. Kamps, M.; Bouten, W.; Seijmonsbergen, A.C. LiDAR and Orthophoto Synergy to optimize Object-Based Landscape Change: Analysis of an Active Landslide. *Remote Sens.* **2017**, *9*, 805. [CrossRef]
54. Ortuño, M.; Guinau, M.; Calvet, J.; Furdada, G.; Bordonau, J.; Ruiz, A.; Camafort, M. Potential of airborne LiDAR data analysis to detect subtle landforms of slope failure: Portainé, Central Pyrenees. *Geomorphology* **2017**, *295*, 364–382. [CrossRef]
55. Francioni, M.; Salvini, R.; Stead, D.; Coggan, J. Improvements in the integration of remote sensing and rock slope modelling. *Nat. Hazards* **2018**, *90*, 975–1004. [CrossRef]
56. Giordan, D.; Manconi, A.; Tannant, D.D.; Allasia, P. UAV: Low-cost remote sensing for high-resolution investigation of landslides. In Proceedings of the IEEE International Geoscience and Remote Sensing Symposium (IGARSS), Milan, Italy, 26–31 July 2015. [CrossRef]
57. Mancini, F.; Castagnetti, C.; Rossi, P.; Dubbini, M.; Fazio, N.L.; Perrotti, M.; Lollino, P. Coastal rocky cliffs: From UAV close-range photogrammetry to geomechanical finite element modeling. *Remote Sens.* **2017**, *9*, 1235. [CrossRef]
58. Vanneschi, C.; Eyre, M.; Francioni, M.; Coggan, J. The use of remote sensing techniques for monitoring and characterization of slope instability. *Procedia Eng.* **2017**, *191*, 150–157. [CrossRef]
59. Liu, Q.; Kieffer, D.S.; Bitenc, M. Three-dimensional UAV-based photogrammetric structural models for rock slope engineering. In Proceedings of the IAEG/AEG Annual Meeting, San Francisco, CA, USA, 17–21 September 2018; Shakoor, A., Cato, K., Eds.; Volume 1, pp. 283–287.
60. Colarossi Mancini, A. *Storia di Scanno e guida nella Valle del Sagittario*; Vecchione, Ed.; Italy, 1921; p. 382.